Department of Aeronautics
Imperial College London

Analysis of Ship Hydrodynamics Using the Overlapping Domain Decomposition Level Set Method

Keith Lam
Final Year MEng Project
February – May, 2007

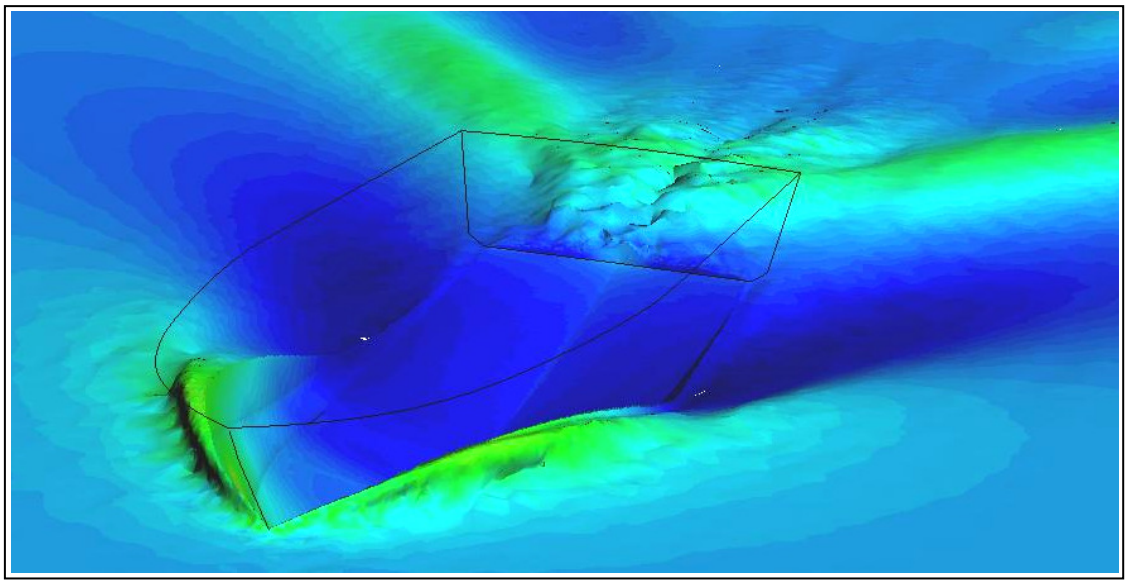

Written at

Compass Ingeniería y Systemas
CIMNE - The International Centre for Numerical Methods in Engineering

UPC – Universitat Politecnica de Catalunya

Barcelona, Spain.

Summary

This report investigates the free surface capture of the Overlapping Domain Decomposition Level Set Method (ODDLS). The CFD software Tdyn is used to carry out computations in unison with GiD a pre/post processor to prepare the model and to analysis data. The Arbitrary Lagrangian-Eulerian method is also applied to allow deformation of the model mesh to allow the hull to sink and trim and to optimise free surface capture.

The offshore patrol vessel NT-130 developed by Navtec in Chile is the focus of the computations. Experimental towing tank data for still water conditions was compared to Tdyn results to asses its performance. Also, data from tests in wave conditions is presented in this report.

Acknowledgements

I would like to offer my sincere gratitude to Professor J. García and Mr A. Valls for their continuous support, asistance and patience during this project. Also, without the invaluable experience from the GiD team, testing would not have progressed so smoothly and achieving sucessful results.

My appreciation goes to Navtec for offering me the opportunity to carry out research with their NT-130 hull and providing me with experimental data for validation.

Finally I would like to thank Professor E. Oñate at CIMNE and Professor M. Graham of Imperial College London for their encouragement and supervision throughout the last four months.

Contents

Index of Figures

Glossary

Sink and Trim – Movement of the hull when given two degrees of freedom pitch and vertical displacement.

Bow – The frontmost part of the hull

Stern – The rear-most part of the hull

Portside – The left side of the boat when facing the Bow

Starboard – The right side of the boat when facing the Bow

Waterline – An imaginary line circumscribing the hull that matches the surface of the water when the hull is stationary.

Midship – The midpoint of the LWL (see below) half-way from the forwardmost point on the waterline to the rear-most point on the waterline.

Baseline – An imaginary reference line used to measure vertical distances from. It is usually located at the bottom of the hull.

Length Overall (LOA) – The extreme length from one end to the other

Length on the Waterline (LWL) – The length from the forwardmost point of the waterline measured in profile to the stern-most point of the waterline.

Beam (B) – The width of the hull.

Depth (D) – The vertical distance from the bottom of the hull to the uppermost edge at the side.

Draft (d) – The vertical distance from the bottom of the hull to the waterline.

Freeboard (FB) – The difference between depth and draft.

Longitudinal Centre of Buoyancy (LCB) – The longitudinal distance from a point of reference to the centre of the displaced volume of water when the hull is not moving. Note that the Longitudinal Centre of Gravity or centre of the weight of the vessel must align with the LCB when the hull is in equilibrium.

1.0 Introduction

1.1 Background

In the field of computational fluid dynamics, the analysis on two immiscible (non-mixing) fluids is vastly complex compared to that of a single infinite fluid. The coupling between incompressible flow equations and the free surface condition causes many problems. The analysis of the interaction between two different fluids is of interest to various areas of engineering such as Marine hull design, injection moulding and combustion.

A great deal of effort has been put into developing methods to tackle this problem. Especially at CIMNE the International Centre of Numerical Methods Engineering in Barcelona, where researchers are using Lagrangian and Eulerian approaches to develop their methods. A newly developed method of capturing the free surface known as the Overlapping Domain Decomposition Level Set Method (ODDLS) will be the focus of this project. Implemented using Tdyn from COMPASS Ingenieria y Sistemas, the computations and analysis will serve to validate the ODDLS method.

A Pre/Post Processor developed in-house at CIMNE called GiD v8.0 will be used to prepare and analyse data for the computations.

1.2 Aims and Objectives

Whilst validating the capabilities and accuracy of the ODDLS method, this project will serve to provide CFD analysis data for an Offshore Patrol Vessel NT-130 designed by Navtec.

The series of computations in various configurations will include:

- Investigation into the Effect of the Centre of Gravity Location
- Fixed Hull Analysis in Still Water
- Sink and Trim Analysis in Still Water
- Damping Effect by the Increase in Time step
- Sink and Trim Analysis in Still Water

Towing tank longitudinal resistance data has been provided by Navtec and will be the basis of comparisons with Tdyn results.

If time permits, a Catamaran of a Bi-Wigley configuration will also be tested to analyse the sink and trim in still water.

2.0 Theory

2.1 Interface Modelling Methods

Interface modelling is relevant to a wide range of engineering applications such as the analysis of slamming for planning hulls in waves, sloshing of fluids in tanks and casting of molten materials. The free surface is an interface between two immiscible fluids where the properties of one is negligible relative to the other. A common analysis is in hydrodynamics with water and air where the density of water is approximately one thousand times greater then that of air.

Decades of research and development has been spent on developing an efficient, accurate and reliable means of simulating large free surface deformation. The coupling of incompressible flow equations and the free surface condition makes this difficult to accurately simulate compared to infinite fluid problems. The free surface condition or otherwise known as the kinematic condition states that a particle on the free surface will always remain on the surface. The problem is that neither the geometry nor position of the free surface is known.

There are two main approaches to free surface modelling; interface-tracking and interface-capturing.

Interface Tracking

The interface tracking method is a Lagrangian approach that adapts itself to the geometry of the interface throughout its evolution with time. Smooth Particle Hydrodynamics Method (SPH) and Particle Finite Element Method (PFEM) are examples of this approach [5].

The free surface is treated as a boundary of the computational domain where the kinematic and dynamic boundary conditions are applied. This method allows the mesh to adapt with large topological displacements of free surface. Therefore, it is particularly useful for analysing the boundary layer close to the free surface. However, it can be computationally expensive as the mesh requires updating after every time step and it is difficult to accurately apply a mass continuity condition.

Interface Capturing

The interface capturing method is an Eulerian approach which uses a fixed mesh that does not adapt to a moving interface. It requires some intuition by the user to predict where to apply areas of fine mesh to capture large topological changes at the free surface. This method considers both fluids as a single effective fluid where its properties change at the interface [5].

The Level Set Method and Volume of Fluid Method (VOF) are examples of this approach. They can accurately model breaking waves, surface tensions and complex geometry at the free surface. However the ‘jump’ in fluid properties at the interface is difficult to model as this is constantly moving, separating and reconnecting. Therefore the imposition of exact boundary conditions at the interface is usually simplified.

The computational software used in this project Tdyn, incorporates interface capturing based on the level set method with a Lagrangian-Eulerian approach. This allows the mesh to deform, giving the hull freedom to sink and trim (displacement in vertical direction and pitch) whilst capturing the free surface.

2.2 Level Set Method

The Level Set Method was first devised by S. Osher and J. A. Sethian (1988, Jnl. Comp. Phys) [6]. This was an approach to modeling the evolution of an interface Γ that bounds an open region Ω in two or three dimensions. The interface can be between two immiscible fluids such as liquid and gas, in this instance the interactions of water and air are investigated. The motion of Γ under a velocity field ν is tracked by embedding it as a level set function of the signed distance away from the interface. The velocity ν depends upon the position, time, interface geometry and the external physics.

Other numerical methods attempt to track the moving interface with a layer of interconnected marker points. A known velocity ν indicates their changes in positions corresponding to the moving interface. Problems arise with this method when deformation of the interface becomes complex, in the case of bow waves and turbulent wakes. When marker points move over each other the links are crossed or separated, interconnections become disorganized and are very difficult to track. Also, the model can become unstable and divergence occurs as an acute curvature develops. Due to small errors in the position of marker points, much greater errors in the modeling of the contour result.

The level set method does not focus on tracking the interface itself. It takes the original curve and constructs a surface that is a signed distance from a point on the interface to the xy plane. The cone shaped surface figure 2.1 intersects the xy plane on the location of the curve. This cone is known as the level set function where the input is a point on the xy plane and the output is its signed distance from the interface. The red front indicates the position of the interface where $\phi = 0$ known as zero level set. The sign of the level set function indicates which fluid the point resides.

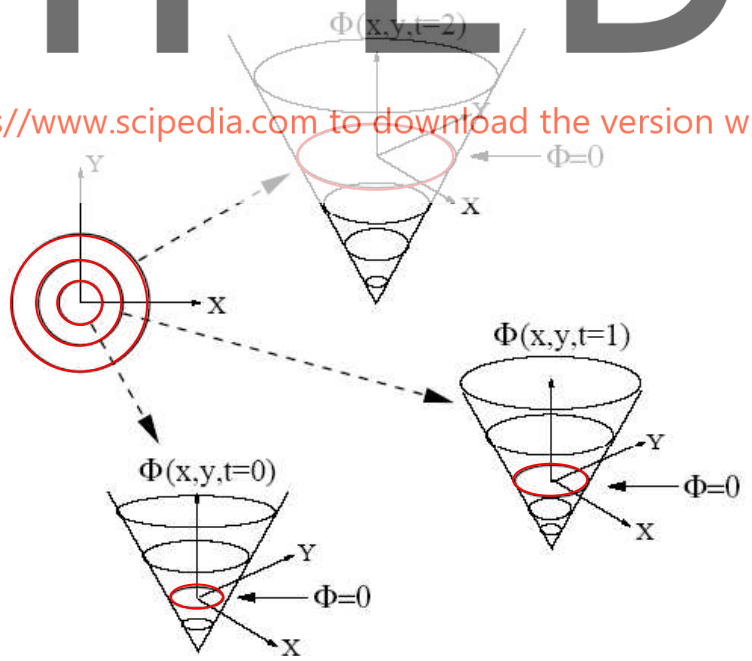

Figure2.1: Transformation of front motion into initial value problem

Initial Value Formulation

The geometry of an interface is captured by moving the level set function on the xy plane which can rise, fall and expand. The zero level set is taken to find the location of the front at t=0. This is referred to as an "initial value formulation" because the initial position of the interface provides information for its evolution through time.

The advantage of using this method is that even as the interface becomes highly contorted the level set function will remain well behaved [6]. Thus, allowing the straightforward modelling of topological changed such as wave breaking and merging. Also, this method can be trivially extended from two to three dimensions.

The level set function $\phi(x,y,t)$ has the following properties:

$$\begin{aligned} &\phi(x,y,t) > 0 \ \ for \ \ (x,y) \ outside \ fluid \ (water) \\ &\phi(x,y,t) = 0 \ \ for \ \ (x,y) \in \Gamma(t) \\ &\phi(x,y,t) < 0 \ \ for \ \ (x,y) \ inside \ fluid \ (water) \end{aligned} \tag{2.2.1}$$

The initial value of the interface is constructed by taking the signed distances of $\phi(x,y,t=0)$ from the xy plane. Therefore, at all later times the interface can be captured by locating $\Gamma(t)$ where ϕ become zero. The motion of the front can be determined by convecting the values of ϕ in a velocity field v. While the initial point on the interface is $\phi(x,y,t) = 0$ at a particular position on the xy plane. To determine the behavior of this point in time and space, the derivative of the function $\phi(x,y,t)$ is found. Therefore, the level set function that describes the evolution of the interface is

$$\frac{\partial \phi}{\partial t} + v_j \frac{\partial \phi}{\partial x_j} = 0. \tag{2.2.2}$$

The interface boundary is defined by

$$\Gamma(t) = \{(x,y) | \phi(x,y,t) = 0\}. \tag{2.2.3}$$

The region Ω (t) is bounded by $\Gamma(t) = \{(x,y) | \phi(x,y,t) > 0\}$ and the exterior are defined by $\Gamma(t) = \{(x,y) | \phi(x,y,t) < 0\}$.

The unit normal N to $\Gamma(t)$ is given by $$N = -\frac{\nabla \phi}{|\nabla \phi|} \tag{2.2.4}$$

.

The mean curvature κ of $\Gamma(t)$ is defined as $$\kappa = -\nabla\left(\frac{\nabla \phi}{|\nabla \phi|}\right) \tag{2.2.5}$$

The Dirac's delta function concentrated on an interface is $$\delta(\phi)|\nabla \phi| \tag{2.2.6}$$

Coupling of the level set method with external physics

The interface analysis for this project involves external physics where numerous methods are available, including front tracking, phase-field methods and the volume of fluid (VOF) approach. The level set analysis for incompressible flow and flows with singular vorticity will be discussed.

The two-phase Navier Stokes incompressible flow coupled the level set method with external physics [6].

$$u_t + u \cdot \nabla u + \frac{\nabla p}{\rho} = g + \frac{\nabla \cdot (2\mu D)}{\rho} + \frac{\delta(\phi)\sigma\kappa N)}{\rho} \qquad (2.2.3)$$
$$\nabla \cdot u = 0$$

Where:

$u = (u, v, \omega)$ – fluid velocity
p – pressure
$\rho = \rho(\phi)$ – piecewise constant fluid density
$\mu = \mu(\phi)$ – piecewise constant fluid viscosity
g – gravitational acceleration
D – viscous stress tensor
σ – surface tension coefficient
κ – curvature of the interface
N – unit normal
$\delta(\phi)$ – delta function

This equation is coupled to the front motion with the level set function equation (2.2.2) that describes the evolution of the interface with $v = u$.

As intricate topological interface motions occur, the level set formulation provides regularisation by blocking interface self-intersection. Two and three dimension unstable vortex motion can be computed without regularisation, other then in discrete approximation to the delta function $\delta(\phi)$. Know as "topological regularization" any curve or surface is viewed as the level set of a function, when it evolves with an unstable velocity field, divergence is prevented. For example, if a curve is tracked through a figure of eight pattern, the level set captured curve would pinch off and stabilise before this occurs [6].

Consider Euler equations in two dimension incompressible flow

$$\omega_t + u \cdot \nabla \omega = 0$$
$$\nabla \times u = \omega \qquad (2.2.4)$$
$$\nabla \cdot u = 0.$$

Vorticity initially concentrated on a set characterised by the level set function ϕ

Vortex path: $\omega = H(\phi)$ (2.2.5)

Vortex sheet: $\omega = \delta(\phi)$, $\left(\text{strength of sheet } \frac{1}{|\nabla \phi|}\right)$ (2.2.6)

Vortex sheet dipole: $\omega = \frac{d}{d\phi}\delta(\phi) = \delta'(\phi)$. (2.2.7)

As ϕ satisfies a simple advection equation and u and v can be easily recovered.

2.3 Statement of Problem

The velocity and pressure fields of two incompressible and immiscible fluids moving in a two or three dimension domain Ω between the time interval (0,T], can be described by the incompressible Navier Stokes equations for multiphase flows. This is also known as the non-homogeneous Navier Stokes equations [5]. In general marine applications the range of velocities that are analysed are low enough to assume the fluids to be incompressible. Therefore, the Navier Stokes equations become independent of the energy equations, reducing a variable.

$$\begin{gathered} \partial_t \rho + \nabla(\rho u) = 0 \\ \partial_t(\rho u) + \nabla \cdot (\rho u \otimes u) - \nabla \cdot \sigma = \rho f \\ \nabla \cdot u = 0 \end{gathered} \tag{2.3.1}$$

Where:

ρ – fluid density field u – velocity field σ – Cauchy stress tensor

The Cauchy stress tensor is defined by

$$\begin{gathered} \sigma = -p\mathrm{I} + \tau \\ \tau = \mu(\nabla u + \nabla u^T) \end{gathered} \tag{2.3.2}$$

.

Where:

μ – dynamic viscosity I – identity matrix

While the following problem has a moving interface inside the domain, all sub-domains and functions are time dependent.

For all $t \in [0,T)$, let $\Omega_1(t) = \{(x,y) \in \Omega | x \text{ is Fluid}_1\}$ be part of the domain Ω occupied by fluid 1 and let $\Omega_2(t) = \{(x,y) \in \Omega | x \text{ is Fluid}_2\}$ be part of the domain Ω occupied by fluid 2. Therefore $\Omega_1(t)$ and $\Omega_2(t)$ are two disjoint sub-domains of Ω. Then

$$\Omega = \mathrm{int}\left(\overline{\Omega_1(t) \cap \Omega_2(t)}\right) \text{ for all } t \in (0,T] \tag{2.3.3}$$

where 'int' denotes the topological interior (points inside the domain) and the over bars indicates the topological adherence (all points inside and on the boundary of domain) of a given set. The equations (2.3.1) must be completed with the necessary initial and boundary conditions below. For multiphase incompressible flows, the density is not considered to be constant in $\Omega \times (0,T]$ and ρ, μ fields can be defined as

$$\rho(x,y,t), \mu(x,y,t) = \begin{cases} \rho_1, \mu_1 & (x,y) \in \Omega_1(t) \\ \rho_2, \mu_2 & (x,y) \in \Omega_2(t) \end{cases} \text{ for all } (x,y,t) \in \Omega \times (0,T] \tag{2.3.4}$$

Therefore the Level Set can now be defined as

$$\phi(x,y,t) = \begin{cases} d(x,y,\Gamma(t)) & (x,y) \in \Omega_1(t) \\ 0 & (x,y) \in \Gamma(t) \\ -d(x,y,\Gamma(t)) & (x,y) \in \Omega_2(t) \end{cases} \tag{2.3.5}$$

Where $d(x, y, \Gamma(t))$ is the distance of the point (x, y) to the interface between the two fluids, denoted by $\Gamma(t)$, at time t. From (2.3.5) the surface is obtained as

$$\Gamma(t) = \{(x, y) \in \Omega | \phi(x, y, t) = 0\}. \tag{2.3.6}$$

Now, it is possible to write the definition as

$$\rho, \mu = \begin{cases} \rho_1, \mu_1 & \phi > 0 \\ \rho_1, \mu_1 & \phi < 0 \end{cases} \tag{2.3.7}$$

Rewriting the density fields in terms of the level set function ϕ

$$\rho(x, y, t) = \rho(\phi(x, y, t)) \quad \text{for all } (x, y, t) \in \Omega x(0, T] \tag{2.3.8}$$

The density derivatives can be written as

$$\begin{aligned} \partial_t \rho &= d_\phi \rho \cdot \partial_t \phi \\ \nabla \rho &= d_\phi \rho \cdot \nabla \phi. \end{aligned} \tag{2.3.9}$$

Inserting relation (2.3.9) into for first equation of system (2.3.1) gives

$$\begin{gathered} \partial_t \rho + \nabla(\rho u) \underset{\nabla \cdot u = 0}{=} \partial_t \rho + (u \cdot \nabla)\rho = d_\phi \rho \cdot \partial_t \phi + d_\phi \rho \cdot (u \cdot \nabla)\phi = 0 \\ d_\phi \rho [\partial_t \phi + (u \cdot \nabla)\phi] = 0 \end{gathered} \tag{2.3.10}$$

The multiphase Navier Stokes problem (2.3.1) is therefore equivalent to solving the following system of equations

$$\begin{aligned} \partial_t(\rho u) + \nabla \cdot (\rho u \otimes u) - \nabla \cdot \sigma &= \rho f \\ \nabla \cdot u &= 0. \end{aligned} \tag{2.3.11}$$

coupled with the equation

$$\partial_t \phi + (u \cdot \nabla)\phi = 0. \tag{2.3.12}$$

Equation (2.3.12) defines the transport of the level set function due to the velocity field obtained by solving the equations (2.3.11). Therefore, the free surface capturing problem can be described by these equations. The interface between the two fluids is defined by the zero value of the level set function ϕ. It is possible to prove, assuming the variables of the problem are sufficiently smooth that the system given by equations (2.3.11) and (2.3.12) has a unique global solution [13].

The boundary conditions of equations (2.3.11) and (2.3.12) can be denoted by an over-bar the prescribed values and by n the normal to the boundary are

$$\begin{aligned} u &= \bar{u} \quad \text{on} \quad \Gamma_D \\ n\cdot\sigma &= \bar{t} \quad \text{on} \quad \Gamma_N \\ n\cdot u = u_n, \quad & \left.\begin{aligned} n\cdot\sigma\cdot g &= \bar{t}_1 \\ n\cdot\sigma\cdot s &= \bar{t}_2 \end{aligned}\right\} \quad \text{on} \quad \Gamma_M \end{aligned} \tag{2.3.13}$$

The boundary $\partial\Omega$ of the domain Ω has been split into three disjoint sets Γ_D and Γ_N where the Dirichlet and Neumann boundary conditions are imposed respectively. Also, mixed conditions are imposed on Γ_M . These conditions are usually applied when wall functions are used for modeling the behavior of flow closed to solid walls. The vectors g and s in (2.3.13) span the space tangent Γ_M . Due to equation (2.3.12) being hyperbolic, only boundary conditions must be imposed in the inlet denoted by Γ_{inlet} , defined as

$$\Gamma_{inlet} = \{(x,y)\in\Gamma \,|\, n(x,y)\cdot u(x,y) < 0\}. \tag{2.3.14}$$

Then the boundary condition for equation (2.3.12) is

$$\phi = \bar{\phi} \quad \text{on} \quad \Gamma_{inlet}. \tag{2.3.15}$$

Therefore, the initial conditions for the problem are

$$\begin{aligned} u &= u_0 \quad \text{in} \quad \Omega, \\ \phi &= \phi_0 \quad \text{in} \quad \Omega. \end{aligned} \tag{2.3.16}$$

The initial value of ϕ is defined by the initial position of the interface. Using the definition (2.3.5), ϕ_0 can be computed as the signed distance to the initial interface position where $\Gamma(0) = \{(x,y)\in\Omega \,|\, \phi(x,y,0) = 0\}$.

2.4 Overlapping Domain Decomposition Level Set Method (ODDLS)

This new approach to the level set method introduces the overlapping domain decomposition concept to increase the accuracy of free surface capture and the resolution for governing equations in the interface of the two fluids [5]. Thus allowing the use of an unstructured mesh with larger elements and does not require a surface to be drawn at the level of the interface. This method can be simplified to solve only one of the two interacting fluids. Perfect for hydrodynamic applications where the effect of air on a hull is negligible relative to water.

Free surface capturing is based on the solution of a level set style of equation, while the solution of the Navier-Stokes equations is based on an implicit monolithic second order method. This scheme is derived by splitting the momentum equation in a similar way as in an implicit fractional step method [5].

This is an illustration of the domain partition showing the overlapping domains $\tilde{\Omega}_1$ and $\tilde{\Omega}_2$.

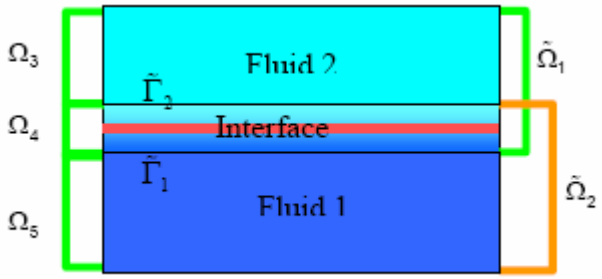

Figure 2.2: Geometrical Domain Decomposition

The following is a detailed view of the interface with the free surface intersecting triangular mesh elements.

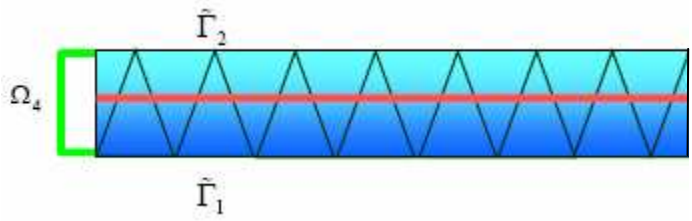

Figure 2.3: Sketch of mesh elements intersected by the interface

The finite element partition of domain Ω is,

$$K = \bigcup_{e=1}^{\#K} \left(N^e, K^e, \Theta^e \right) \tag{2.4.1}$$

Where:

N^e – element nodes
K^e – element spatial domain
Θ^e – element shape function
$\#K$ – total number of elements in the partition

Now assume that K satisfies the following approximation property,

$$dist\left(\partial\Omega, \partial\left(\bigcup_{e=1}^{\#K} K^e \right) \right) \leq \max_{1 \leq e \leq \#K} \left\{ diam\left(K^e \right) \right\} \tag{2.4.2}$$

for a fixed time t, $t \in (0, T)$.

The domain is split into three disjoint sub domains Ω_3, Ω_4 and Ω_5, in such a way that $\Omega_3(t) = \bigcup_e K_3^e$ and $\Omega_5(t) = \bigcup_e K_5^e$. Where K_e^3 and K_e^5 are the elements of the finite element partition K, such that all their points satisfy for all $x \in K_3^e \left| \phi(x, y, t) > 0 \right.$ and for all $x \in K_5^e \left| \phi(x, y, t) < 0 \right.$ respectively. The geometrical domain decomposition is completed with

$$\Omega_4 = \Omega \setminus (\Omega_3(t) \cup \Omega_5(t)) \tag{2.4.3}$$

The two overlapping domains are defined from this partition.

$$\tilde{\Omega}_1(t) = \mathrm{int}\left(\overline{\Omega_3(t) \cup \Omega_4(t)}\right), \qquad \tilde{\Omega}_2(t) = \mathrm{int}\left(\overline{\Omega_4(t) \cup \Omega_5(t)}\right). \tag{2.4.4}$$

As $\partial\tilde{\Omega}_i$, i=1, 2 are the boundaries of the domain $\tilde{\Omega}_i$

$$\partial\tilde{\Omega}_i = \Gamma_{iD} \cup \Gamma_{iN} \cup \Gamma_{iM} \cup \tilde{\Gamma}_i. \tag{2.4.5}$$

The domain decomposition technique is the Dirichlet Neumann method where Γ_{iD}, Γ_{iN} and Γ_{iM} are the Dirichlet, Neumann and mixed boundary respectively. There are two restrictions for the boundary condition on $\tilde{\Gamma}_i$ which originates from the presence of an interface in the domain:

1. Fluid velocities must be compatible at the interface.
2. The jump condition must be satisfied on Γ.

The Dirichlet Neumann approach fulfills both restrictions. The Dirichlet conditions are applied on $\tilde{\Gamma}_1$ where we make use of the compatibility of velocities at the interface:

$$u_1 = u_2 \qquad \text{on } \tilde{\Gamma}_1 \tag{2.4.6}$$

Neumann conditions are applied on $\tilde{\Gamma}_2$ which makes use of the jump boundary condition, with a traction vector $\tilde{t}$ such that:

$$n_1 \cdot \sigma_2 = \tilde{t} \qquad \text{on } \tilde{\Gamma}_2 \tag{2.4.7}$$

Here $\tilde{t}$ must ensure the jump boundary condition is maintained, therefore:

$$p_1 n = p_2 n + \gamma \kappa n \qquad \text{on } \Gamma \tag{2.4.8}$$

Details of the computation of $\tilde{t}$ can be found in [5]. A characteristic of this method is its dependence on the mesh size to accurately capture topological changes in the interface. A fine mesh near the free surface and a course mesh away from the area of interest can reduce the number of iterations required to obtain a converged global solution.

2.5 Finite Increment Calculus

Despite decades of intense research, few efficient, accurate and reliable means of analysing incompressible flow with large free surface deformations have been developed. Problems caused by instabilities from high value convective terms in the momentum equations and those induced by the difficulty of satisfying the incompressibility condition are common. Much focus has been on the stabilized numerical methods to overcome these problems in incompressible flow analysis.

Numerous techniques based on the Galerkin and finite element methods (Galerkin FEM) have attempted to avoid instabilities. The standard Galerkin variational form of the momentum and mass balance equation is extended with adequate residual based terms in order to achieve a stabilised numerical scheme. These include:

- The streamline Petrov-Galerkin (SUPG)
- The Galerkin least square (GLS)
- The Taylor-Galerkin
- Characteristic Galerkin
- Characteristic based split (CBS)
- Pressure gradient operator
- Subgrid scale (SS)
- Finite Increment Calculus (FIC)

The finite calculus (FIC) approach is based on invoking the balance of fluxes in a fluid domain of finite size, where additional terms are introduced to the differential equations of momentum and mass balance [3]. Therefore stabilisation is provided for the discrete equations obtained via the standard Galerkin FEM and overcomes the instabilities of the convective and incompressible terms. Thus, low order finite elements such as linear interpolating triangles and tetrahedra can be used with equal order approximations for the velocity and pressure approximations.

Finite Calculus Method

The FIC method is introduced in this section with a convection-diffusion model problem in a 1D domain Ω of length L illustrated in the figure 2.4.

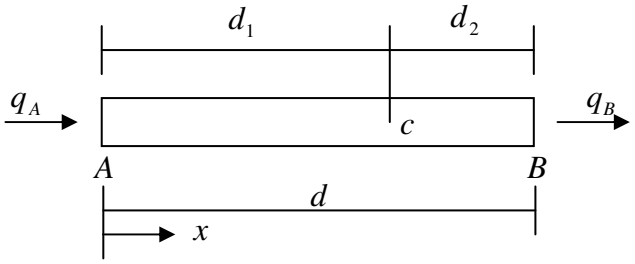

Figure 2.4: Equilibrium of fluxes in a balance domain of finite size.

The equation of balance of fluxes in a subdomain Ω of length d can be written as

$$q_A - q_B = 0, \tag{2.5.1}$$

where q_A and q_B are the incoming and outgoing fluxes at points A and B. The flux defined as

$$q = u\phi - k\frac{d\phi}{dx}, \tag{2.5.2}$$

includes both convective and diffusive terms where:

ϕ – transport variable u – velocity k – diffusivity of material

The second order Taylor series of the fluxes q_A and q_B about point C

$$q_A = q_C + d_2 \frac{dq}{dx}\Big|_C + d_1^2 \frac{d^2q}{dx^2}\Big|_C + O\left(d_1^3\right), \tag{2.5.3}$$

$$q_B = q_C + d_2 \frac{dq}{dx}\Big|_C + d_2^2 \frac{d^2q}{dx^2}\Big|_C + O\left(d_2^3\right). \tag{2.5.4}$$

Substituting equations (2.5.3) and (2.5.4) into (2.5.1) gives

$$\frac{dq}{dx} - \underline{\frac{h}{2}\frac{d^2q}{dx^2}} = 0, \tag{2.5.5}$$

where $h = d_1 - d_2$ and all the derivatives are computed at point C assuming the balance domain has a finite size. The underlined term in equation (2.5.5) comes from the FIC formulation, which introduces the characteristic length h. The distance h can be interpreted as a free parameter depending on the location of point C. Numerical schemes with enhanced stability properties can therefore be derived from equation (2.5.5).

Applying equation (2.5.5) to the convection-diffusion problem up to second order derivatives of ϕ, its explicit form can be written as

$$-u\frac{d\phi}{dx} + \left(k + \frac{uh}{2}\right)\frac{d^2\phi}{dx^2} = 0. \tag{2.5.6}$$

The modified equation (2.5.6) introduces an additional diffusion term commonly known as artificial diffusion into the convection-diffusion equation via the FIC method. Equation (2.5.6) can be extended to account for source effect and the FIC equation can be written in compact form as

$$r - \underline{\frac{h}{2}\frac{dr}{dx}} = 0, \tag{2.5.7}$$

with

$$r = -u\frac{d\phi}{dx} + \frac{d}{dx}\left(k\frac{d\phi}{dx}\right) + Q, \tag{2.5.8}$$

where the external force is Q. A modified Neumann boundary condition derived by invoking balance of fluxes in a domain of finite size next to the boundary Γ_q in the FIC method is

$$k\frac{d\phi}{dx} + q_p - \underline{\frac{h}{2}r} = 0 \quad \text{at} \quad \Gamma_q. \tag{2.5.8}$$

The standard Dirichlet condition prescribing the value of ϕ at the boundary Γ_ϕ completes the definition of the problem. The underlined terms in (2.5.7) and (2.5.8) provide stabilization in the discrete solution of the problem.

Finite Calculus Formulation of Viscous Incompressible Flows

The finite calculus form of the governing differential equations for a three dimensional viscous incompressible flow can be written in an Eulerian frame of reference [3].

Momentum

$$r_m - \underline{\frac{1}{2} h_j \frac{\partial r_{mi}}{\partial x_j}} = 0 \quad \text{in} \quad \Omega \quad i, j = 1,2,3 \tag{2.5.9}$$

$$r_{mi} = \rho\left(\frac{\partial u_i}{\partial t} + u_j \frac{\partial u_i}{\partial x_j} \right) + \frac{\partial p}{\partial x_i} - \frac{\partial s_{ij}}{\partial x_j} - b_i \tag{2.5.10}$$

Mass Balance

$$r_d - \underline{\frac{1}{2} h_j \frac{\partial r_d}{\partial x_j}} = 0 \quad \text{in} \quad \Omega \quad j = 1,2,3 \tag{2.5.11}$$

$$r_d = \frac{\partial u_i}{\partial x_i} \quad i, j = 1,2,3 \tag{2.5.12}$$

Where:

Ω – analysis domain

u_i – velocity along the ith global axis

ρ – density of fluid

p – absolute pressure

b_i – body forces

s_{ij} – viscous deviatoric stresses

The viscous deviatoric stresses is related to the viscosity μ by the following expression

$$s_{ij} = 2\mu\left(\dot{\varepsilon}_{ij} - \delta_{ij} \frac{1}{3} \frac{\partial u_k}{\partial x_k} \right), \tag{2.5.13}$$

where δ_{ij} is the Kronecker delta and the strain rates $\dot{\varepsilon}_{ij}$ are

$$\dot{\varepsilon}_{ij} = \frac{1}{2}\left(\frac{\partial u_i}{\partial x_j} + \frac{\partial u_j}{\partial x_i} \right), \tag{2.5.14}$$

The FIC boundary conditions are

$$n_j \sigma_{ij} - t_i + \frac{1}{2} h_j n_j r_{mi} = 0 \quad \text{on} \quad \Gamma_t \tag{2.5.15}$$

$$u_j - u_j^p = 0 \quad \text{on} \quad \Gamma_u \tag{2.5.16}$$

The initial condition is $u_j = u_j^0$ for $t = t_0$.

Where:

t_i – surface traction on boundary Γ_t

u_j^p – is the prescribed displacement on boundary Γ_u

n_j – components of normal vector to the boundary

σ_{ij} – total stresses given by $\sigma_{ij} = s_{ij} - \delta_{ij} p$

The equations presented in this section are the basis of deriving stabilised FEM for solving incompressible Navier Stokes equations. The underlined FIC term in (2.5.9) overcomes the instabilities due to convective terms in the momentum equations and those of (2.5.11) suppress instabilities due to the incompressibility constraint.

Free Surface Wave Equations

On the free surface Γ_ϕ there are two conditions that must be sustained at any time [3]:

1. The pressure that approximates normal traction must equal the atmospheric pressure p_A and the tangential tractions must equal zero.
2. The particles of the fluid must belong to the free surface.

The first condition can be fulfilled trivially by imposing $p = p_A$ on Γ_ϕ during the calculation of nodal pressures. The second can be written in FIC form whilst neglecting time stabilizing effects .

$$r_\phi - \underline{\frac{1}{2} h_\phi \frac{\partial r_\phi}{\partial x_j}} = 0 \quad \text{on} \quad \Gamma_\phi \quad j = 1,2 \tag{2.5.17}$$

$$r_\phi = \frac{\partial \phi}{\partial t} + \upsilon_i \frac{\partial \phi}{\partial x_i} - \upsilon_3 \quad i = 1,2 \tag{2.5.18}$$

Where the relative velocity is

$$\upsilon_j = u_j - u_j^m \ . \tag{2.5.19}$$

For equation (2.5.17) the underlined term provides stabilization for the solution of the highly convective and non-linear equation defining the evolution of the free surface elevation. It is a popular assumption that the transom flow occurring above specific speed has a singularity for the solution of the following free surface equation.

$$\phi^{n+1} = \phi^n - \Delta t \left[\upsilon_i^{n+1} \frac{\partial \phi^n}{\partial x_i} - \upsilon_3^{n+1} - \frac{h_{\phi_i}}{2} \frac{\partial r_\phi^n}{\partial x_i} \right], \quad i = 1,2 \ . \tag{2.5.20}$$

Stabilized Integral Forms

The weighted residual form of the momentum and mass balance equations is therefore

$$\int_\Omega \delta u_i \left[r_{mi} - \frac{h_j}{2}\frac{\partial r_{mi}}{\partial x_j} \right] d\Omega + \int_{\Gamma_t} \delta u_i \left(\sigma_{ij} n_j - t_i + \frac{h_j}{2} n_j r_{mi} \right) d\Gamma = 0 , \tag{2.5.21}$$

$$\int_\Omega q \left[r_d - \sum_{i=1}^{n_d} \tau_i \frac{\partial r_{mi}}{\partial x_i} \right] d\Omega = 0 , \tag{2.5.22}$$

where δu_i and q are arbitrary weighted functions representing virtual velocities and virtual pressure field respectively. Assuming r_{mi} to be negligible on the boundaries and integrating by parts, the resulting momentum and mass balance equations are

$$\begin{aligned} &\int_\Omega \left[\delta u_i \rho \left(\frac{\partial u_i}{\partial t} + u_j \frac{\partial u_i}{\partial x_j} \right) + \frac{\partial \delta u_i}{\delta x_j} \left(\mu \frac{\partial u_i}{\partial x_j} - \delta_{ij} \rho \right) \right] d\Omega - \int_{\Omega_t} \delta u_i b_i d\Omega \\ &- \int_{\Gamma_t} \delta u_i t_i d\Gamma + \int_{\Omega_t} \frac{h_j}{2} \frac{\partial \delta u_i}{\delta x_j} r_{mi} d\Omega = 0 \end{aligned} \tag{2.5.23}$$

$$\int_\Omega q \frac{\partial u_i}{\partial x_i} d\Omega + \int_\Omega \left[\sum_{i=1}^{n_d} \tau_i \frac{\partial q}{\partial x_i} r_{mi} \right] d\Omega = 0 . \tag{2.5.24}$$

Prior to integrating the parts the following identity was used in the derivation of the viscous terms in the equation (2.5.23).

$$\frac{\partial s_{ij}}{\partial x_i} = 2\mu \frac{\partial \varepsilon_{ij}}{\partial x_j} = \mu \frac{\partial^2 u_i}{\partial x_j \partial x_j} \tag{2.5.25}$$

Convective and Pressure Gradient Projections

The computation of residue terms can be simplified by introducing convective and pressure gradient projections c_i and π_i.

$$c_i = r_{mi} - \rho u_j \frac{\partial u_i}{\partial x_j} \tag{2.5.26}$$

$$\pi_i = r_{mi} - \frac{\partial \rho}{\partial x_i} \tag{2.5.27}$$

Substituting c_i and π_i into (2.5.23) and (2.5.24) respectively giving additional variables. The system of equations is now augmented by forcing the residue r_{mi} to vanishes for both convective and pressure gradient projections giving

$$\int_{\Omega}\left[\delta u_i\rho\left(\frac{\partial u_i}{\partial t}+u_j\frac{\partial u_i}{\partial x_j}\right)+\frac{\partial \delta u_i}{\delta x_j}\left(\mu\frac{\partial u_i}{\partial x_j}-\delta_{ij}\rho\right)\right]d\Omega-\int_{\Omega_t}\delta u_i b_i d\Omega$$
$$-\int_{\Gamma_t}\delta u_i t_i d\Gamma+\int_{\Omega_t}\frac{h_k}{2}\frac{\partial(\delta u_i)}{\delta x_k}\left(\rho u_j\frac{\partial u_i}{\partial x_j}-c_i\right)d\Omega=0 \tag{2.5.28}$$

$$\int_{\Omega} q\frac{\partial u_i}{\partial x_i}d\Omega+\int_{\Omega}\sum_{i=1}^{n_d}\tau_i\frac{\partial q}{\partial x_i}\left(\frac{\partial p}{\partial x_i}+\pi_i\right)d\Omega=0 \tag{2.5.29}$$

$$\int_{\Omega}\delta c_i\rho\left(\rho u_j\frac{\partial u_i}{\partial x_j}+c_i\right)d\Omega=0 \quad \text{no sum in } i, \tag{2.5.30}$$

$$\int_{\Omega}\delta\pi_i\tau_i\left(\frac{\partial p}{\partial x_i}+\pi_i\right)d\Omega=0 \quad \text{no sum in } I, \tag{2.5.31}$$

Where $i, j, k = 1, n_d$. In (2.5.30) and (2.5.31), δc_i and $\delta\pi_i$ are appropriate weighting functions with the ρ and τ_i weights added for convenience. To ensure the stabilization terms in the integral equations (2.5.28) to (2.5.31) have a residual form that vanishes at the exact solution, we must account for the convective and pressure gradient projections which enforces the consistency of the formulation.

2.6 Arbitrary Lagrangian-Eulerian Formulation (ALE)

In the analysis of the free surface for a planning hull in still water and in waves the movement of some parts of the domain is necessary. In the mobile parts of the domain it is more appropriate to use a Lagrangian formulation of the equations and update the spatial discretization after every time step [5]. However, in the fixed areas, the standard Eulerian formulation is more suitable. The finite calculus form of the governing differential equations can be formulated using the Arbitrary Lagrangian-Eulerian technique giving

$$r_{mi}=\rho\left(\frac{\partial u_i}{\partial t}+\left(u_j-u_j^m\right)\frac{\partial u_i}{\partial x_j}\right)+\frac{\partial p}{\partial x_i}-\frac{\partial s_{ij}}{\partial x_j}-b_i, \tag{2.5.32}$$

$$r_d=\frac{\partial u_i}{\partial x_i}, \tag{2.5.33}$$

$$r_\phi=\frac{\partial\phi}{\partial t}+\left(u_j-u_j^m\right)\frac{\partial\phi}{\partial x_i}=0. \tag{2.5.34}$$

Where u_j^m is the relative velocity between the local axis fixed to the fluid particle and the global reference system.

3.0 Software

3.1 Tdyn

The Overlapping domain decomposition level set method validated in this project is implemented by the computational software Tdyn. It is the main tool for analysis carried out at the engineering consultancy, Compass Ingenieria y Systemas, Barcelona.

"Tdyn is a fluid dynamic (CFD) simulation environment based on the stabilized Finite Element Method. Tdyn works with number of different turbulence models and sophisticated tools for simulating problems of species advection, heat transfer in fluids and solids, as well as free surface among others. Tdyn also includes fully integrated pre/post-processing modules. Tdyn is highly flexible in defining physical properties of the model, boundary conditions, through user-defined functions that can make Tdyn a tool with large variety of applications. Moreover, Tdyn includes wizard-type utilities to make analyses definitions fast and easy to do. Finally, Tdyn can be easily adapted to specific needs allowing a simple and automated analysis process."

Compass Ingenieria y Systemas website [15]

The ILES turbulence model [5, 7, 9] was used for the simulations during the testing phase of the project, it is most suited to the transom stern of this planning hull. Three particular modules within Tdyn were utilised for this free surface flow simulation:

- RANSOL was used for incompressible and slightly compressible real fluids with viscosity and turbulence.
- ALEMESH allowed the deformation of the mesh for the hull to sink and trim in still water or waves.
- ODDLS simulates and tracks the free surface interaction between air and water.

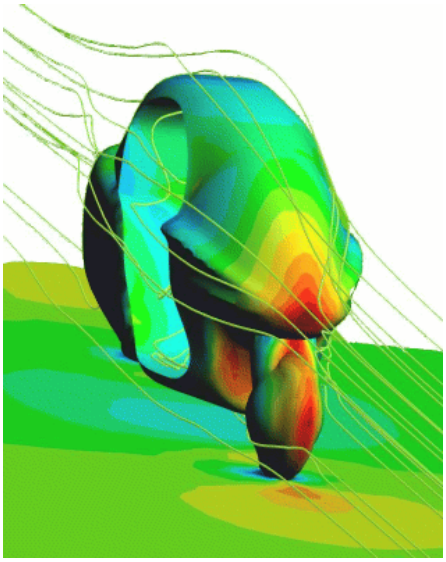

Figure 3.1: Dynamic pressure distribution and flow streamlines over motorcycle.

3.2 GiD 8.0 Pre/Post Processor

Tdyn employs the graphical user interface GiD for geometrical modelling, data input and visualisation of results. GiD can handle many situations in solid and structural mechanics, fluid dynamics and heat transfer, using finite element, finite volume and boundary element [14]. GiD is ideal for generating information for engineering analysis including structured/unstructured meshes, boundary/loading conditions, material types, visualisation of results and more. GiD is well suited for use with Tdyn as it can read and write data according to the specific needs of each individual code. This pre/post processor is being continuously developed with latest beta version 8.1.2b.

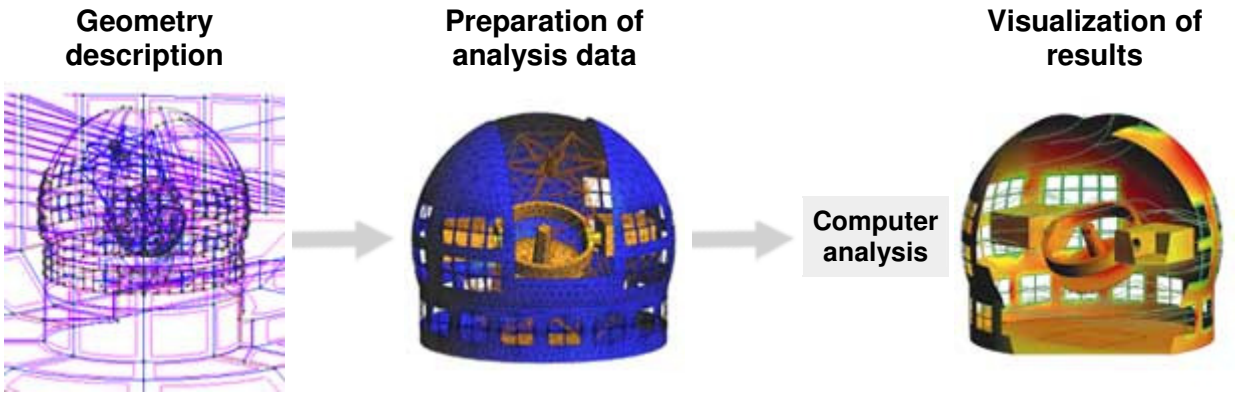

Figure 3.2: Illustration of GiD pre/post processing environment.

To construction and configuration of the model is carried out in the GiD Pre Processor environment. This includes preparing the geometries and meshing. A vital aspect of GiD is that it allows the assignment of unstructured element sizes for lines, surfaces and volumes. This makes it highly versatile in optimising the mesh to achieve a balance between accuracy of results and computation time.

Once the model is ready, information can be sent to the program Tdyn for computation. The Post Processor environment of GiD is used to present data in many different forms of visualisation and also create animations.

FEM: Finite Element Method
FDM: Finite Difference Method
FVM: Finite Volume Method
FPM: Finite Point (meshless) Method

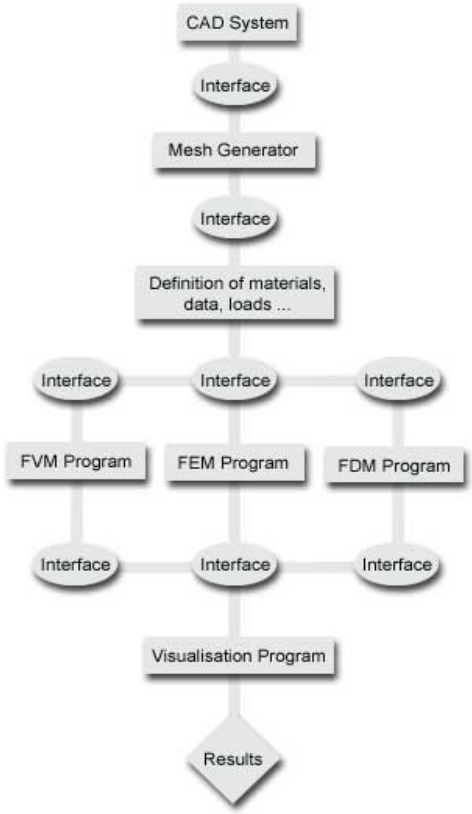

Figure 3.3: Flow diagram of GiD – Tdyn interaction.

4.0 Validation:

Columbian Navy Patrol Vessel NT-130

Figure 4.1: A high speed planning hull of the Columbian Navy.
(Photograph courtesy of Nautatec)

The focus of this series of testing involves the NT-130 semi-displacement hull, designed by Navtec in Chile as an Offshore Patrol Vessel. This has similar configuration to the boat pictured above in figure 4.1, however the NT-130 has an overall length (LOA) of 14m with waterline length (LWL) of 12.5m. With a depth of 2.35m and a beam of 4.0m

The displacement of water for a planning hull remains relatively constant at low speeds or when it is stationary. As it accelerates over a certain speed range, the hull gains sufficient lift to rise above the water. Therefore, the boat displaces less water with a smaller hull wetted area. As a result, the longitudinal viscous (skin friction) and pressure (profile drag) forces are significantly reduced. This is the advantage of a planning hull, as it gains lift the drag is reduces, so with more power it can accelerate at an immense rate.

However, the disadvantage of this design is its instability when travelling through waves, it has little lateral resistance to wave motion, causing pitch and roll oscillations often lifting the propellers out of the water [18]. At sufficiently high speeds, the shallow hull rests on the top of the water and the hull almost jumps from the top of one wave to the next. Consequently, as waves become larger the variation in sink and trim is increased and the effect of slamming as the hull contacts the surface is magnified. This generally causes crew discomfort and in extreme circumstances the pounding can injure passengers and damage the hull or equipment.

Boats with planing hulls are often used for recreational or coastal patrol purposes, where waves are relatively small. However for the NT-130 offshore patrol vessel it is likely to encounter the larger waves on the high seas. Therefore in this situation a semi-displacement hull is used, where it can gain lift at high speeds to reduce drag but maintain the stability characteristic of a displacement hull as it can carve through the crest of each wave. Some disadvantages of this design are its requirement for larger and more powerful engines that consume fuel at a relatively higher rate.

The NT-130 utilises a deep V design at the Bow which evolves into a regular V at the Midship and a Transom stern. The following images in figure 4.2 & 4.3 of the NT-130 hull without deck configurations are captured from the pre-process environment of GiD.

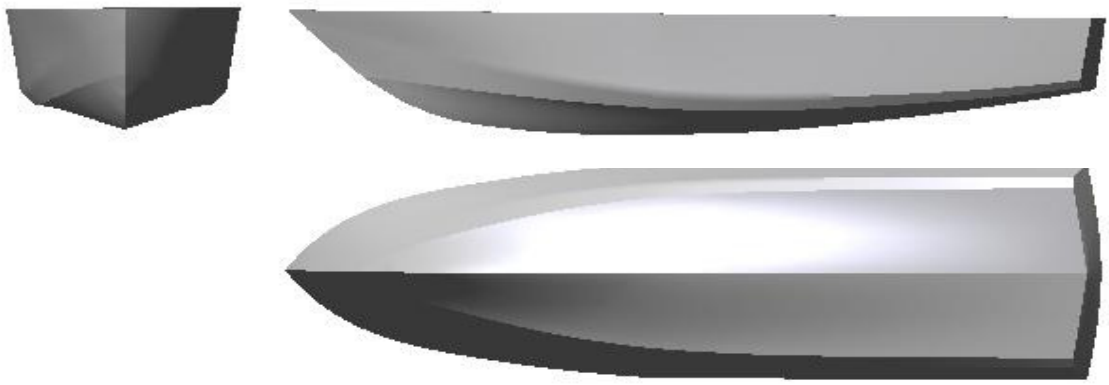

Figure 4.2: Front, side and base view of the NT-130 hull Offshore Patrol Vessel.

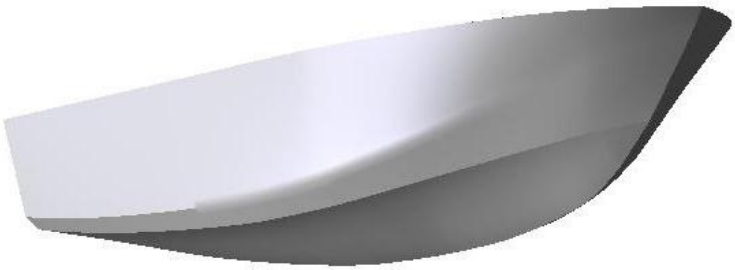

Figure 4.3: Isometric view of the NT-130 Offshore Patrol Vessel.

The deep V at the bow of the hull allows the forward section to slice through the waves displacing the water at the crest of the wave gradually to reduce slamming [19]. The flat Transom stern allows the aft section to squat slightly, keeping the propeller and rudder deep in the water to optimize energy transfer for propulsion and steering. Figure 4.4 shows a stationary scale model of the NT-130 hull in a towing tank. The towing point is visible at some distance above the hull causing a longitudinal downwards pitching moment as towing force increase. This would typically be counteracted by relocating the centre of gravity. Guides forward and aft of the towing point help reduce any lateral rotation of the hull during towing keeping the boat straight.

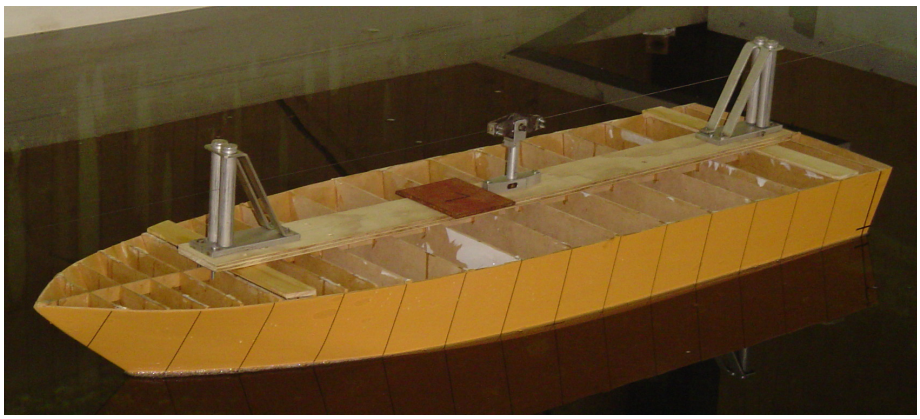

Figure 4.4: Towing Tank Scale Model Stationary in Water (Photograph courtesy of Navtec)

4.1 Initial Testing: Investigation into the Effect of the Centre of Gravity Location

This range of tests is aimed to investigate the effect on the performance of the boat when the location of the centre of gravity (CG) is moved forward or aft. This can be caused by a range of circumstances such as the loading of equipment, passengers or even the change in fuel levels.

Navtec, the designer of the HT-130 hull was not able to provide data regarding the centre of gravity, towing moment or the thrust vector, all of which significantly affects the running trim and sink of the vessel. Also as this boat is still being developed, information regarding this matter is not available on the internet or available publications. Therefore some initiative was taken to explore at least one of these factors (CG) and was expanded to a performance analysis.

Tdyn Model Description

The location of the CG is indicated in this test by its distance from the forward most point of the waterline (origin) when the hull is stationary. During initial testing, the model was run at zero flow velocity at a specific CG setting while given freedom to sink and trim. When analysing the motion data from each simulation, if the hull was found to pitch downwards the CG would be adjusted aft, conversely the CG would be moved forward if the hull was found to pitch upwards. The amount of adjustment was determined by the rate of change in pitch attitude. After 4 iterations when the adjustment was by less then 0.2m the CG or the longitudinal centre of buoyancy of the hull was found to be situated at 6.5m aft of the origin. This position will be used for computations with the freedom to sink and trim in the following sections. However, 6.5m may not match the position used in the towing tank model, as it had to account for the effect of the propeller on the trimming moment.

Longitudinal Centre of Buoyancy (LCB) is the longitudinal distance from a point of reference to the centre of the displaced volume of water when the hull is stationary. The Longitudinal CG of the vessel must align with the LCB when the hull is in equilibrium [19].

It was decided that 7 tests were to be run at Fn = 0.650 (14kts = maximum operating speed), locating the CG at positions 0.5m apart, three forward and three aft of the LCD. This ranged from 5.0m to 8.0m from the origin, providing sufficient scope for investigating more extreme loading conditions during operation. The following figure 4.5 illustrates the locations of the CG relative to the hull plan form.

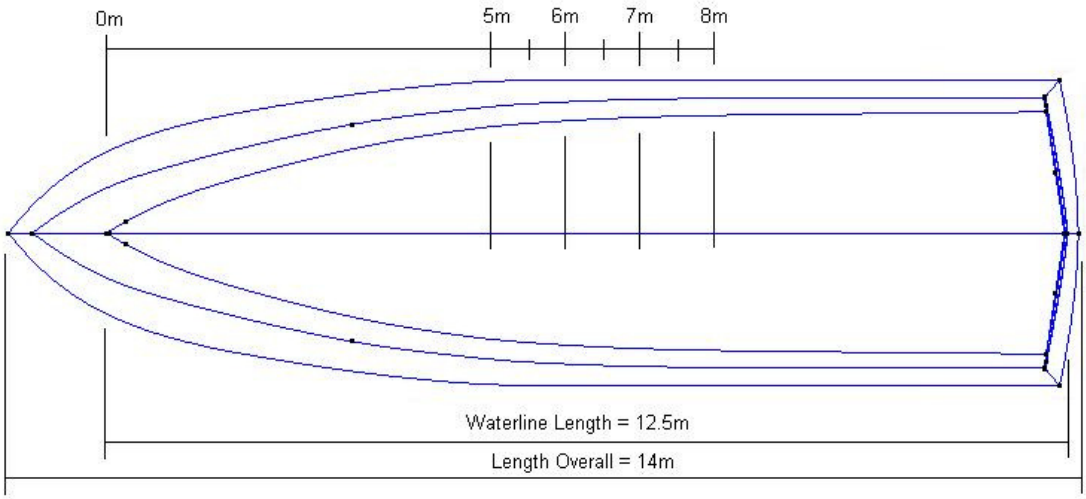

Figure 4.5: Centre of Gravity Locations

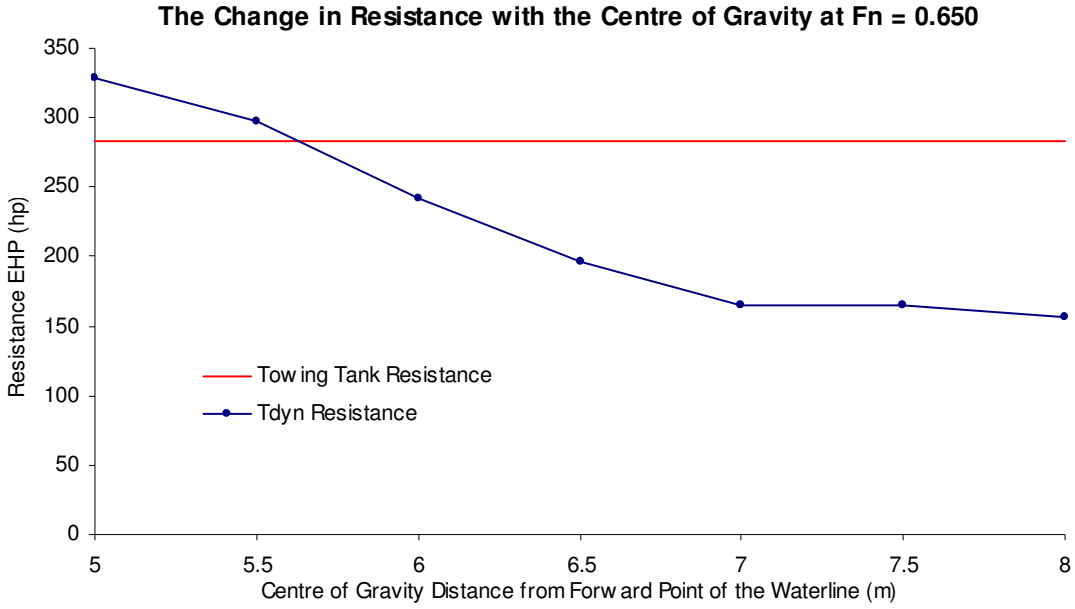

Figure 4.6

The data provided by Navtec represented longitudinal resistance in units of Effective Horsepower (EHP), however Tdyn denotes this with pressure and viscous Forces (N). Therefore, to compare the resistance of the two resting methods the longitudinal viscous (skin friction) and pressure (profile drag) forces were added together and the following conversion factor was used to convert into EHP units.

$$\text{Resistance} = \frac{u(F_p + F_v)}{745}$$

u – velocity (ms^{-1})
F_p – pressure force (N)
F_v – viscous force (N)

(4.1.1)

Figure 4.6 shows the variation in longitudinal resistance as the CG of the boat was adjusted. The red line indicates the EHP resistance measured from the towing tank experiment running at a Froude number of Fn=0.650 equating to 14kts for the full scale Tdyn model. The graph in figure 4.6 shows a general reduction in resistance as the CG of the boat moved backwards. The variation in resistance with CG was relatively linear between 5.0m and 7.0m. However, as the CG moved aft from 7.0m to 8.0m the resistance remained consistent. In appendix A (figure A.1) between 4 – 5 seconds the hull stabilised and the behaviour of the longitudinal pressure force is evident. While the velocity of the flow was identical for every test, the longitudinal viscous force (figure A.2) varied little with small discrepancies due to differences in hull wetted area.

The difference in wetted area for each CG configuration is caused by the sink and trim of the hull. As the boat accelerates, a bow wave and wake develops around the hull. This can be seen in the graphs of appendix A where the data oscillates until after 4 seconds into the simulation where the results converge. The results for the final graph above are only taken only when these topological changes on the surface are fully developed and stabilized. Figure A.3 shows the trim angle of the hull as it accelerates at various CG configurations. When the CG was aligned with the LCB the hull was trimmed at 4.3 degrees pitch up. As expected, once the CG was moved forward of the LCB the trim angle was much lower even negative at -0.18 degrees for the CG 5.0m test. This inhibited the planing effect of the hull and caused the boat to sink by 0.31m beneath the initial level of the free surface, resulting in the high longitudinal resistance of the hull.

Conversely, as the CG was moved aft of the LCB the stabilised trim angle of the hull increased, magnifying the planing effect and thus reducing the wetted area. Although the sinkage was less then tests with CG forward of the LCB, figure A.4 still showed the hull travelling at 0.1m beneath the initial level of the free surface for CG 8.0m. This is originates from the method in which Tdyn measures the height of the boundaries that constructs the hull.

It should be noted that figure A.4 shows the sinkage of tests with CG = 7.0m, 7.5m and 8.0m were comparatively similar with only a few centimetres difference. The planing effect of the hull is optimal at these trim angles, if the boat pitches up further the orientation flat geometry would cause centre of pressure to shift too far backwards reducing the static margin to a point where the boat to flip longitudinally.

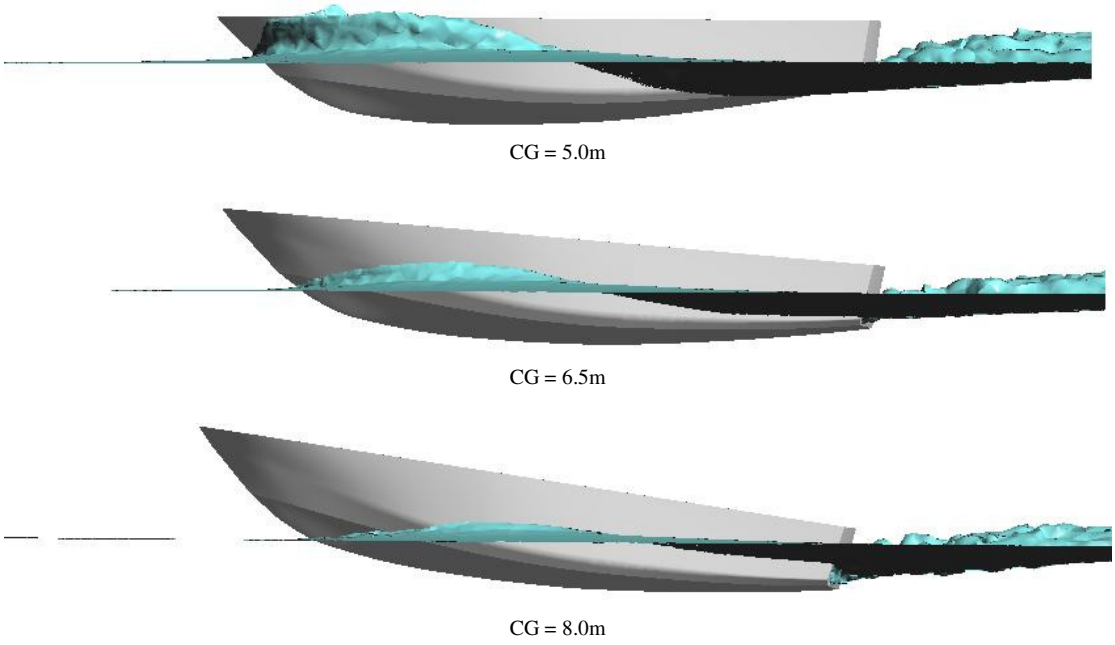

Figure 4.7: Side view of trimmed hulls for various CG locations.

Figure 4.7 illustrates the stabilised attitude of the hull at 5.0m, 6.5m (LCB) and 8.0m, where the attributes of each configuration previously discussed can be observed.

- CG = 5.0m: Negative trim angle of -0.18 degrees with sinkage of 0.31m. It should be noted that the stern of the hull is above the displaced surface of the water possibly exposing the propeller reducing its effect of propelling the boat.

- CG = 6.5m: Trim angle of 4.3 degrees with a sinkage of 0.12m. This configuration will be used for all preceding tests where the hull is free to sink and trim. The effect of the flat transom stern can be clearly seen as it squats beneath the surface of the water, providing good energy transfer for the propellers.

- CG = 8.0m: The hull is trimmed at 8.2 degrees. From the geometry of the stern it is clear that if the boat is operating in this configuration it is possible that the forward view of the crew would be obscured. Also with most of the bow out of the water, the lateral directional stability would be reduced, allowing the hull to yaw when power is applied.

4.2 Fixed Hull Analysis in Still Water

This is the first test that compares results from the towing tank to that of Tdyn with a range of Froude numbers 0.372, 0.465, 0.557 and 0.650 equating to the speeds of 8kts, 10kts, 12kts and 14kts respectively. This test involves fixing all degrees of freedom of the fluid boundaries that forms the hull. Therefore the hull will remain in its original stationary attitude as it moves through the water.

Tdyn Model Description

Figure 4.7 below shows the model used to simulate the NT-130 hull various configurations. Four different mesh sizes were used to optimise data capture and computation time. The fluid boundary of the hull was assigned an unstructured surface element size of 0.1m. This would allow the capture of an accurate boundary layer around the hull. The triangular volume and its surfaces immediately enclose an area that shows the greatest free surface deformation. This layer was not assigned an element size to allow the differentiation between a coarse and fine mesh. The course mesh was given a maximum element size of 0.35m equating to 1.8 million elements and the fine mesh was set to 0.26m with 3.2 elements, the unstructured size transition of both was 0.5. The two volumes forward and aft of the triangular layer represent the free surface where relative little deformation occurs. This volume and its surfaces were given an unstructured element size of 0.5m. The top and bottom volumes represent the areas of air and water furthest away from the hull. The data capture in these volumes does not require a high degree of accuracy, therefore they were assigned unstructured element sizes of 2.0m. Figure B.3 in appendix B illustrates the element size assignment more clearly.

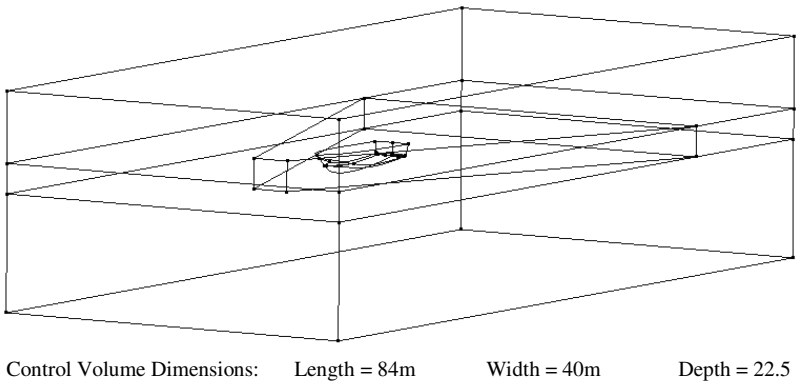

Figure 4.8: GiD model for the NT-130 hull.

The Tdyn conditions RANSOL and ODDLS was applied to the model to form the control volume (CV) and allow the overlapping domain decomposition level set method to be used for the capture of the free surface. Using RANSOL, the initial velocity field for the fluid entrance, side walls and base was fixed for all three axes, lateral y axis and vertical z axis respectively. Also, the initial pressure field was fixed for the fluid exit of the CV. This effectively turned the CV into a towing tank where it had defined side walls, base and fluid flow entrance/exit. The initial ODDLS fix field condition was assigned for the top, bottom surfaces and the flow entrance. The initial (t=0) and reference field of the level set function was defined as

$$0.0 - z \tag{4.2.1}$$

with no reinitialization. Therefore the assigned ODDLS field conditions on the model will be used as a base to calculate boundary conditions.

The following tables provide information regarding the Tdyn settings for this range of tests.

Fluid: Water				
ρ	Density	1000 kg/m3		
μ	Viscosity	0.001 kg/ms		
	Fluid Model	Incompressible		
Fluid Boundary: Hull				
	Boundary Type	YplusWall		
	Mass	None		
	Centre of Gravity	X: 6.5m	y: 0.0m	z: 0.0m
	Radii of gyration	x: 1.0m	y: 4.9m	z: 0.0m
	Displacement Freedom	Fixed		
	Rotation freedom	Fixed		

Tdyn		
N	Number of steps	500
t	Time increment	0.01s
T	Total time	5.00s
	Time integration	Backward Euler
	Turbulence model	ILES
	Movement relaxation factor	0.95
	Simulation run time	6 hrs x 4 = 24 hrs

Results Analysis

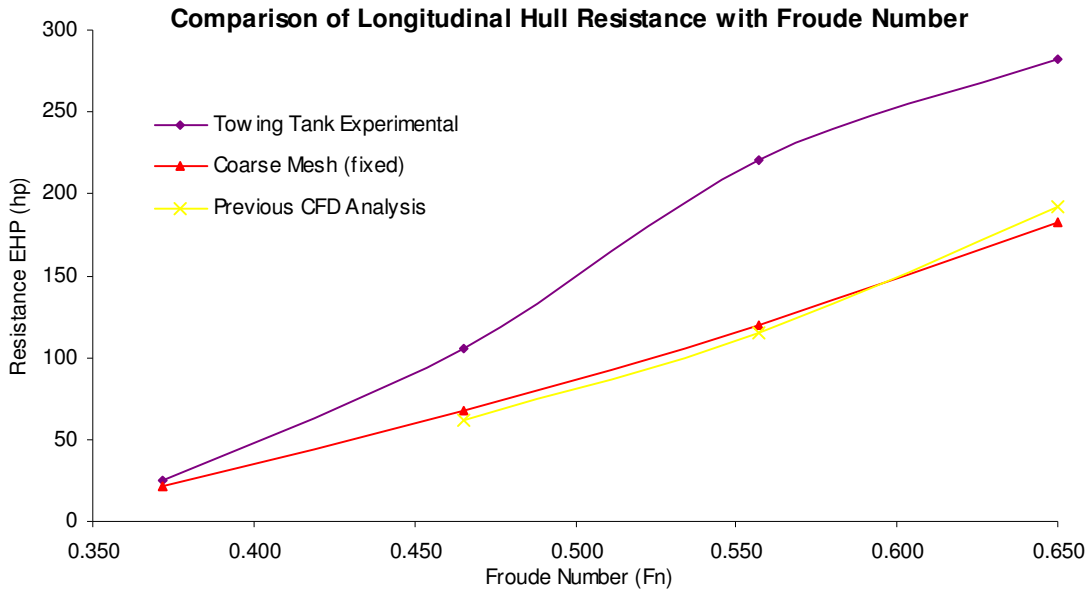

Figure: 4.9

The results of this test are compared in figure 4.8 with the towing tanks experiment and the previous CFD analysis. It is immediately clear that resistance measured from Tdyn is almost identical to that of the previous CFD method that was deemed too inaccurate at high Froude numbers. As the hull remains at zero trim angle and sink height, the forward profile and wetted area remains relatively constant. Therefore, the flow velocity the longitudinal resistance increased without the characteristic jump in the towing tank resistance between Froude numbers of Fn = 0.465 and 0.557.

4.3 Sink and Trim Analysis in Still Water

The main test of this project will be described in this section where the longitudinal resistance characteristics of the hull will be compared with the towing tank experiment that was carried out at a University in Chile. The hull was given two degrees of freedom, pitch and vertical displacement. Initially a coarse mesh with 1.9 million elements was run and after analysing the data, a fine mesh with 3.2 million elements and a reduced time step was simulated.

Tdyn Model Description

This model was set up with the same Tdyn configurations as the previous test with a fixed hull. However, freedom of movement was given for the vertical displacement and pitch rotation components of the hull. This required the assignment of the mass (20.8 tonnes), centre of gravity (6.5m) and pitching radius of gyration calculated in equation 4.3.1 as 35% of the overall length of the hull.

$$\text{Pitching Radius of Gyration} = LOA \times 0.35 \qquad (4.3.1)$$

The Tdyn function ALEMESH was used to assign a mesh deformation condition of "Fix Null" on the CV base, fluid entrance and exit which ignores any other mesh deformation conditions. This gives the model freedom to deform vertically allowing the hull to sink and trim. The mesh deformation is illustrated in figure 4.9 where CV around the hull is clearly bent upwards to allow the boat to trim pitch up. This keeps the areas of high mesh density close to free surface where the greatest topological deformation occurs. The fluid boundary conditions on the hull such as the mass, CG location, radii of gyration and the movement relaxation factor are applied to the ALEMESH condition to influence the deformation of the mesh.

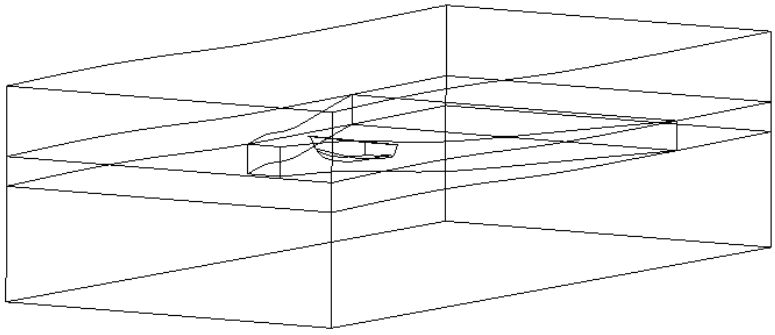

Figure 4.10: ALEMESH sink and trim deformation on NT-130 model.

The following tables provide information regarding the Tdyn settings for the coarse and fine mesh models used for testing.

Fluid: Water				
ρ	Density	1000 kg/m3		
μ	Viscosity	0.001 kg/ms		
	Fluid Model	Incompressible		
Fluid Boundary: Hull				
	Boundary Type	YplusWall		
	Mass	20793kg		
	Centre of Gravity	x: 6.5m	y: 0.0m	z: 0.0m
	Radii of gyration	x: 1.0m	y: 4.9m	z: 0.0m
	Displacement Freedom	Z direction (vertical)		
	Rotation freedom	Y axis (pitch)		

Tdyn (Course mesh)		
N	Number of steps	500
t	Time increment	0.01s
T	Total time	5.00s
	Time integration	Backward Euler
	Turbulence model	ILES
	Movement relaxation factor	0.95
	Simulation run time	10 hrs x 4 = 40hrs

Tdyn (Fine mesh)		
N	Number of steps	1000
t	Time increment	0.005s
T	Total time	5.00s
	Time integration	Backward Euler
	Turbulence model	ILES
	Movement relaxation factor	0.95
	Simulation run time	20 hrs x 4 = 80hrs

The turbulence model ILES was used for this model as it was most suited for the transom stern flow. Also initial testing with a movement relaxation factor of 0.8 saw oscillations in the sink and trim of the hull delay the stabilisation of the wake behind the hull. Therefore the movement relaxation factor was changed to 0.95 and it was found that the flow generally stabilised after 4 seconds. The coarse mesh previously tested with 1.8 million elements used a time step of 0.01s with 500 steps to reach a final simulation time of 5s. However the fine mesh with 3.2 million elements required a smaller time increment of 0.005s to avoid the appearance of negative volumes during the computation. This generally appears when the element size around a wave is small and the deformation of the free surface is too large for Tdyn to track for the specific time step. Therefore Tdyn sees a negative volume in the region of the high free surface deformation and the computation stops.

Results Analysis

The longitudinal resistance for both the coarse and fine mesh simulations are compared with the previous fixed hull test and the towing tanks experiment in figure 4.10.

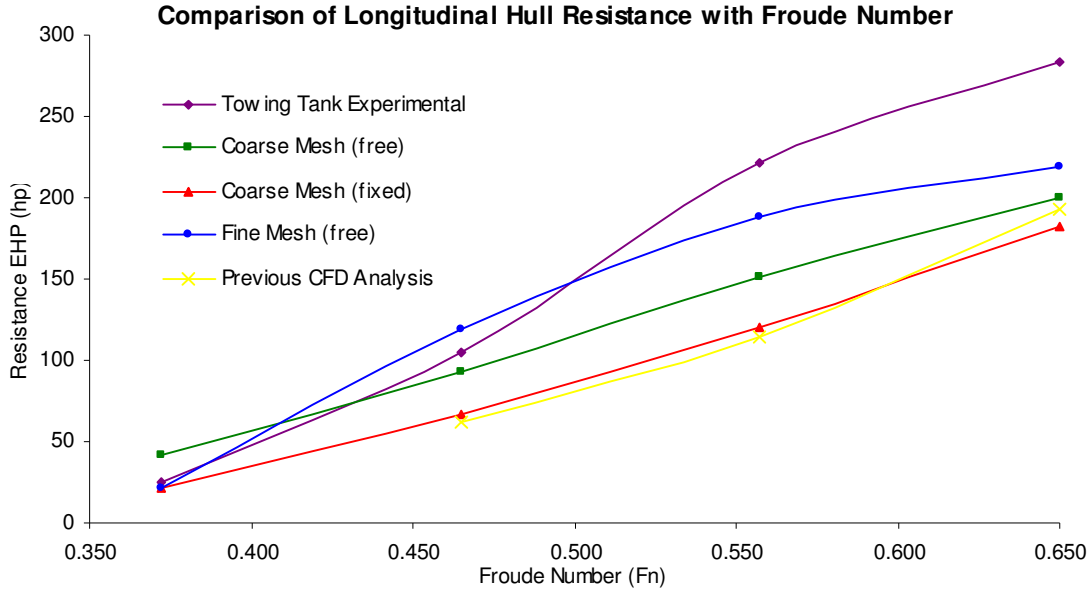

Figure: 4.11

The green curve represents the model with a coarse mesh and a hull free to sink and trim. Its behavior is similar to that of the fixed hull test, however an overall increase in resistance of 30hp. Comparing longitudinal graphs of figures C.3 and B.4 in appendix C and B, it is apparent that the increase in resistance did not come from viscous forces (skin friction). However, looking at figures C.2 and B.3 a marked increase of approximately 2500N in pressure force can be seen for computations at all four Froude numbers. Thus variations in pitch attitude and sinkage do not significantly alter the wetted area of the hull, but the forward profile is significantly increased causing a much higher longitudinal pressure force however.

The blue curve in figure 4.10 represents the fine mesh computation with a hull free to sink and trim. This series of tests provided results that were far more accurate then previous with percentage error to towing tank data of approximately 10% to 22% over the whole range of Froude numbers. On the previous longitudinal viscous force graph for the course mesh free to sink and trim, steps in the results have appeared along the curves of all Froude numbers. However for the fine mesh these steps have become highly oscillatory before the stabilization of the wake. An explanation for this anomaly has yet to be found.

Figure 4.11 and 4.12 shows the fully developed flow of the coarse and fine mesh models respectively, at T = 5s and Fn = 0.650.

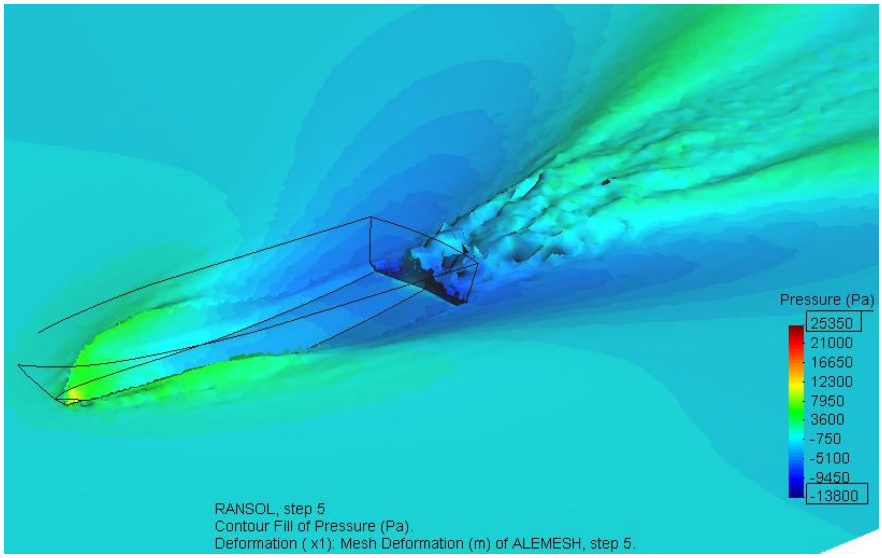

Figure 4.12: GiD flow visualization for coarse mesh model

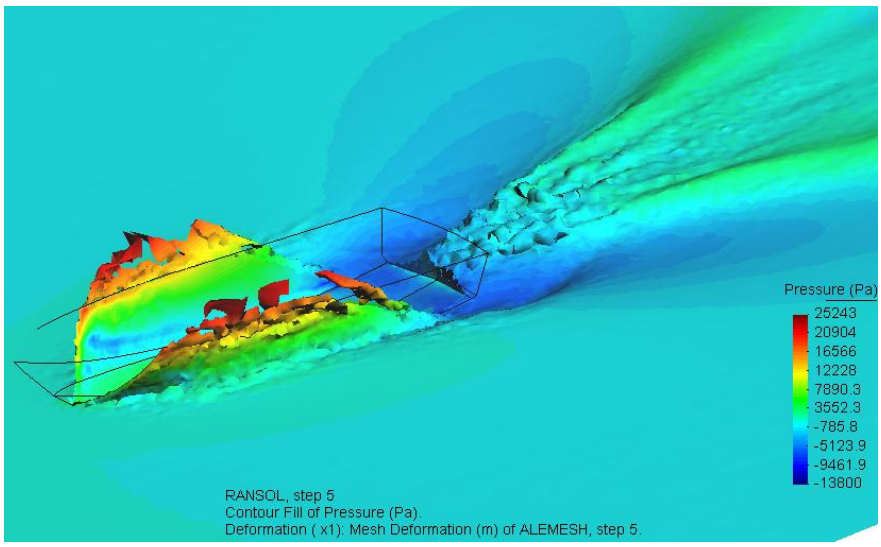

Figure 4.13: GiD flow visualization for fine mesh model

The Arbitrary Lagrangian-Eulerian mesh deformation is demonstrated by the sink and trim of the fluid boundaries of the hull. This is updated every dime step to react to external forces from the freestream flow. Overlapping domain decomposition level set is used to capture the fluid free surface. The capability of ODDLS can be observed by the complex geometry of the bow wave on either side of the hull and fully developed wake diverging aft of the stern. The post process environment of the beta version of GiD 8.1.2B allows the visualization of the free surface geometry with a smooth rendering to overcome some limitations of element size. Finally RANSOL function calculates the pressure of the fluid and can be visualized on the free surface as a spectrum of colours. Reds represent positive high pressures and blues represent negative pressures.

It can be seen in both figures that the areas of greatest pressure is the apex of the deep V bow and the four crests of the bow wave and wake. Conversely the areas of greatest negative pressure are regions of blue behind the bow wave next to the transom stern. These regions are below the initial level of the surface as two deep troughs.

The post process of the fine mesh model uncovered some unexpected free surface characteristics. Most noticeable is the high bow wave where its crest raises higher then the freeboard and extends almost as long as the waterline length (LWL) of the boat. As the photo in figure 4.13 shows, even in waves the bow wave remains below the top of the hull. An explanation for this from other Tdyn experts is that each element within the fluid domain does not have enough mass for gravity to have its full effect. A subsequent effect of this condition is the comparatively deep negative pressure surface on either side of the aft section of the hull. Looking closely at the hull boundaries in figure 4.12, the corners of the transom stern can be seen exposed above the surface of the water. Also, the apex of the deep V bow is comparatively higher then in figure 4.11. This is evident in appendix C figures C.8 and C.9, although the hull is trimmed at an angle 0.5 degrees lower its height is positive above the water 0.18m higher then that of the coarse mesh model.

Although the force data from computations with the fine mesh are more accurate compared to towing tanks results, the free surface behavior provides scope for further investigation.

4.4 Slamming Analysis in Waves

Figure 4.13 shows a towing tank model tested with in wave conditions.

Figure 4.14: Towing tank model in wave conditions (Photograph courtesy of Navtec).

This series of test is the first attempt to use Tdyn to simulate a hull in wave conditions. As this type of dynamic behaviour is beyond the scope of the project, the results will be presented with some comments and observations. The "Linear Theory of Regular Waves" was used to calculate the worst case conditions specific for this hull at four different Froude number settings. As this design will be used by the Spanish navy on the high seas, the "Deep Water" range of formulae was used.

Tdyn Model Description

The alterations made to the original sink and trim model the assignment of an oscillating fluid boundary at the flow entrance as a wave generator and a beach at the exit of the CV to decelerate the flow similar to the configuration in figure 4.14.

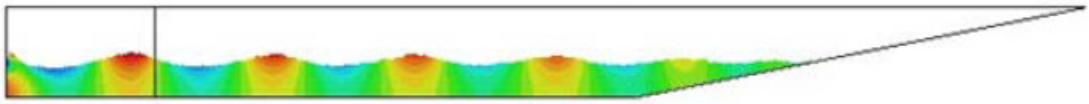

Figure 4.15: Dynamic pressure distribution of waves [5]

A fluid boundary condition was assigned to the flow entrance of the CV, with a sinusoidal function given to the "Velocity X Field" to allow it to oscillate and generate waves. The definition of this function is in equation

$$V_x = V_0 + \frac{1}{2} a\omega \cos[(\omega + kV_0)t] \tag{4.4.1}$$

Where:

V_x – Fluid boundary velocity field

V_0 – Freestream flow velocity

a – Wave amplitude

$\omega = 2\pi/T$ – Wave generator frequency

$T = \sqrt{2\lambda\pi/g}$ – Wave period

$k = 2\pi/\lambda$ – Wave number

λ – Wavelength

t – Time

The amplitude was taken as the total depth (D) of the hull and the wavelength is approximately twice the overall length (LOA). As waves reach the end of the control volume, the oscillations are damped and the flow is decelerated. This is accomplished using a beach effect by applying acceleration fields in the fluid for the vertical and longitudinal directions.

Results Analysis

Figure 4.15 illustrates the motion of the hull in waves at time intervals of 2 seconds from zero to fourteen seconds. The effectiveness of the deep V design at the bow can be observed as the hull carves through the crest of each wave. Also some water can be seen crashing over the freeboard onto the deck of the boat immediately after the crest. This demonstrates capability of the ODDLS method, as the free surface of this body of water can be seen completely separating form the main fluid domain then reattaching at the stern. The slamming effect of this semi-displacement hull is visualised in the last image. Areas of high pressure appear at the apex of the deep V bow as the hull makes contact with the trough of a wave. The last image two images at the bottom of figure 4.15 shows the highly oscillating surface immediately aft of the stern, commonly know as “The Ball” successfully generated.

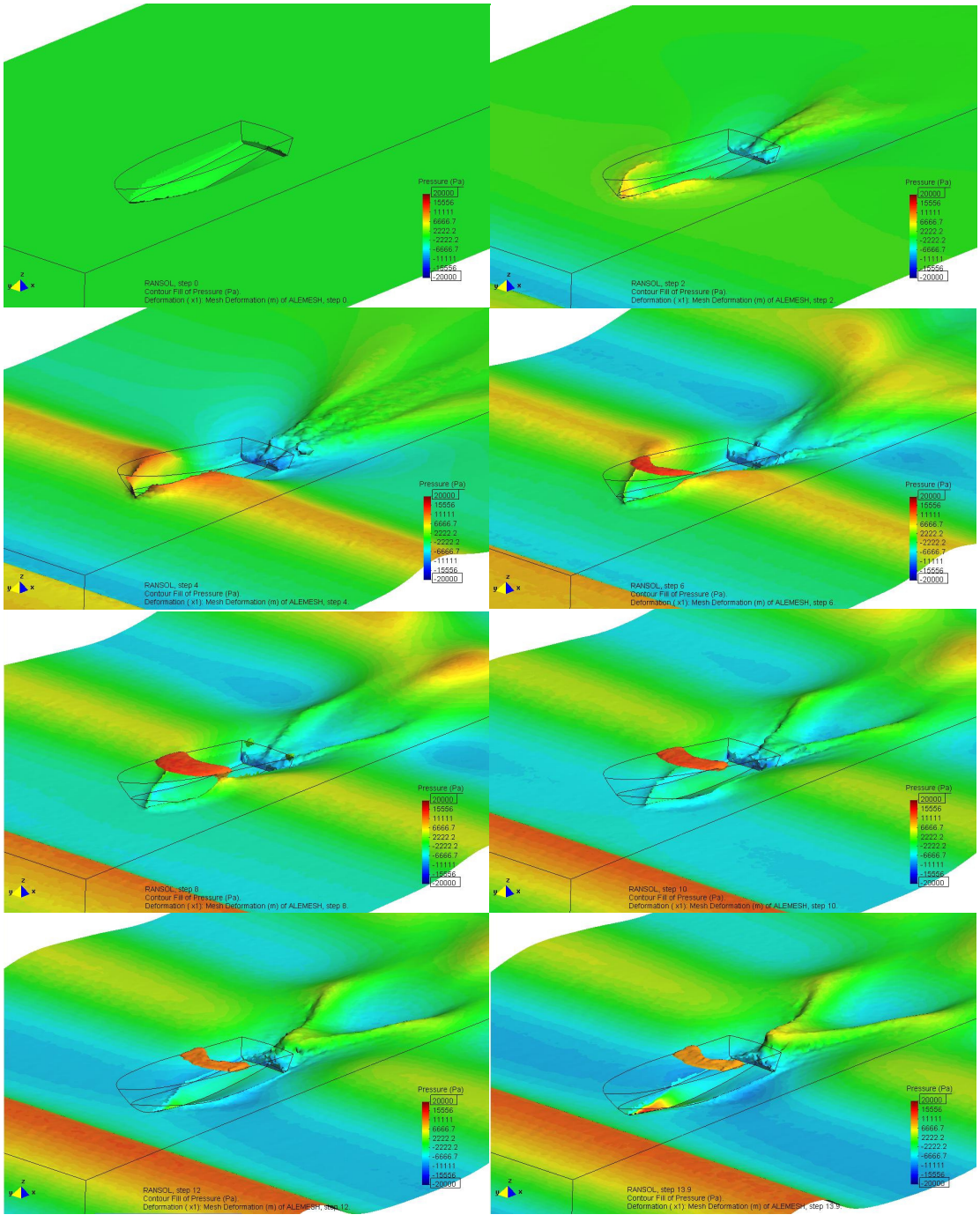

Figure 4.16: Flow visualisation for NT-130 at Fn = 0.650 hull in wave conditions.

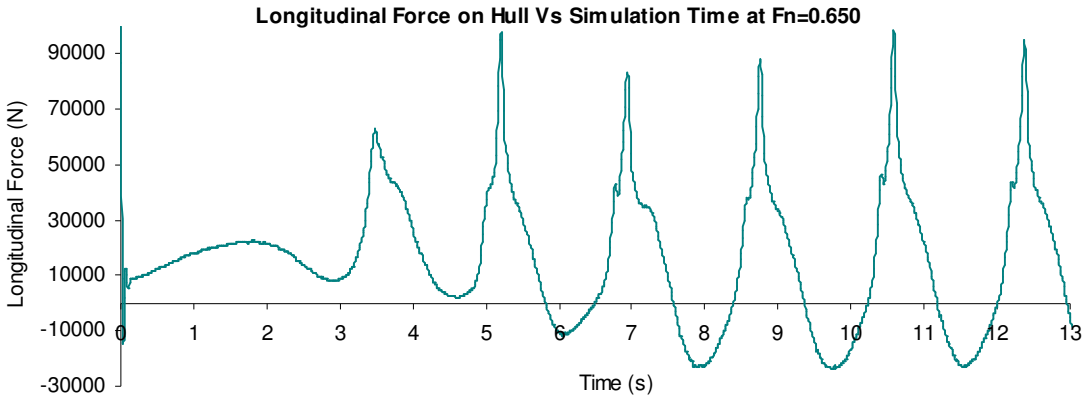

Figure:

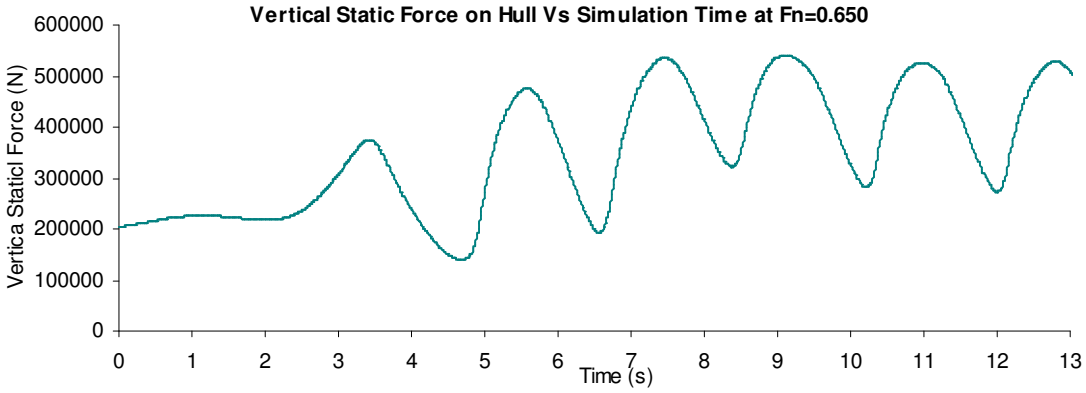

Figure:

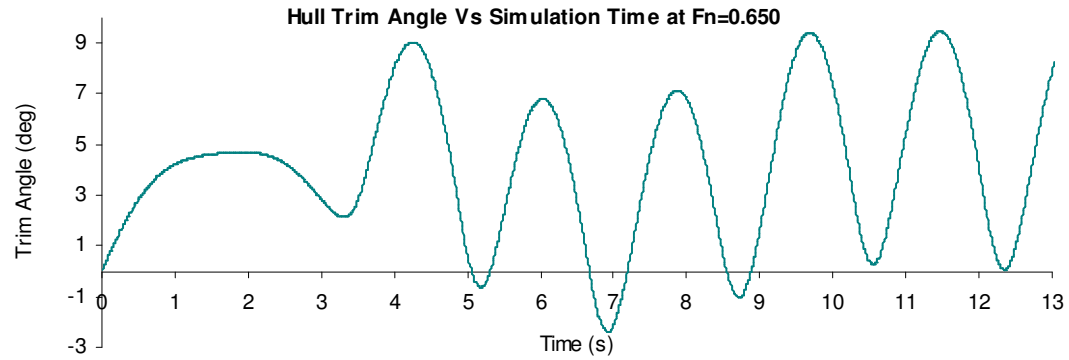

Figure:

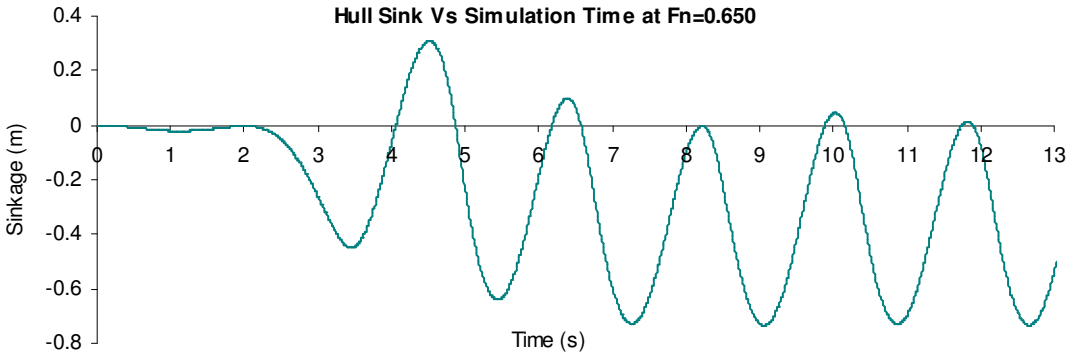

Figure 4.17: Data comparison for Fn = 0.650 in wave conditions.

Figure 4.16 compares longitudinal pressure, vertical static forces with sink and trim data for the simulation visualized in figure 4.15. As the fluid accelerates it takes just below 3 seconds for the first wave to reach the hull. At T = 3.5s the bow makes contact with the first wave causing the pressure and static forces to rise. At T = 4 the hull reacts as the trim angle increases to almost 9 degrees and at T = 4.5 the hull rises to a height of 0.3m above the initial level of the free surface. This cycle continues with slight variations on 6 consecutive waves over a computation of 13.9 seconds. The raw data for this computation can be found in appendix D, figures D.1 – 4.

An experiment to push the boundaries of the wave generating model was carried out by testing the hull at a Froude number of Fn = 2.0 (V_0 = 22.1m/s or 43.1kts). Figure 4.17 below shows the post process images of this simulation. The simulation was set to run for duration of 10 seconds but at 3.9 seconds a negative volume was found in the fluid domain and the computation stopped. After traveling over 2 waves the oscillations were capable of lifting the entire hull out of the waves and pitching almost vertically upwards. The ALEMESH deformation was too large to Tdyn to track and consequently the computation stopped. Figures D.5 – 9 shows the data for this experiment.

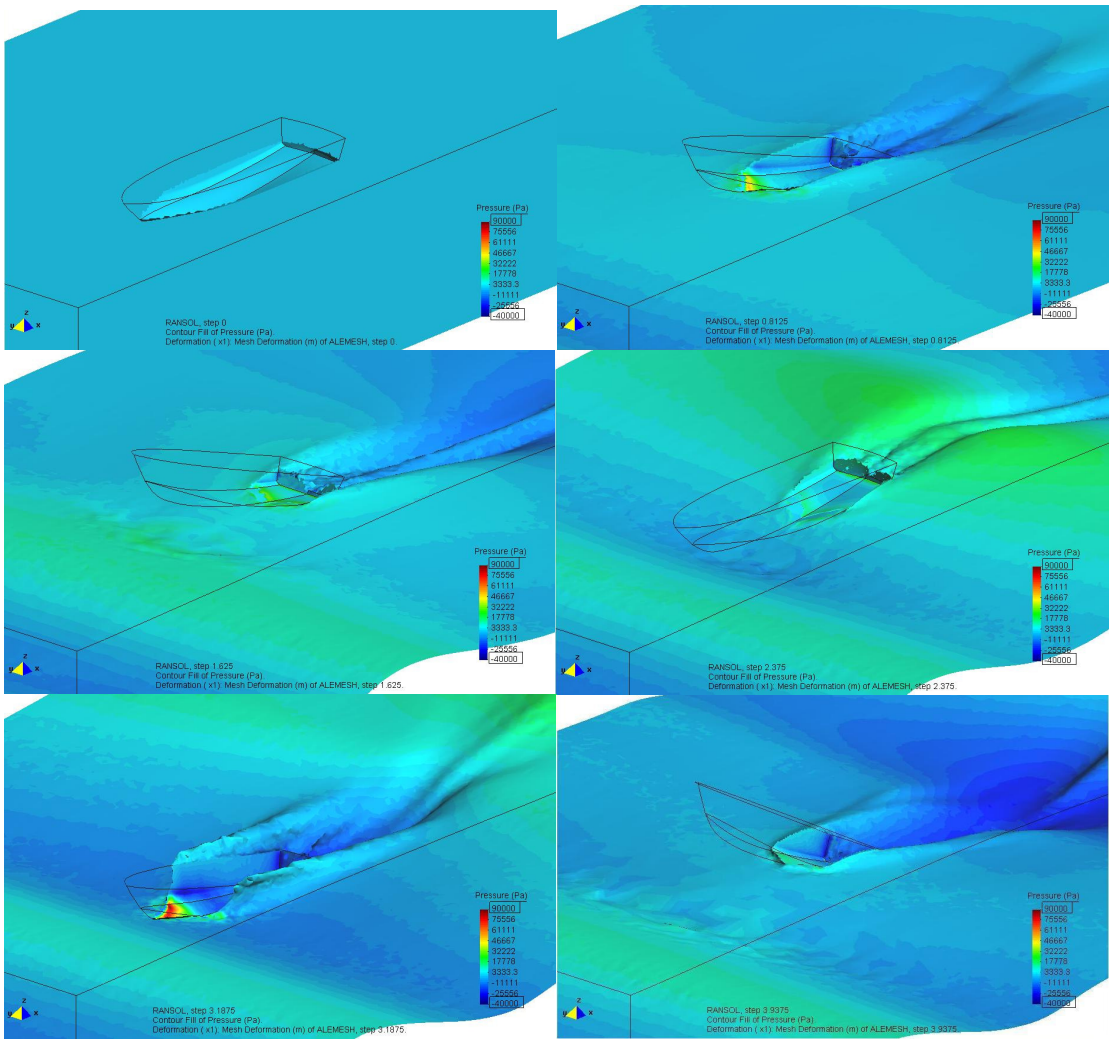

Figure 4.18: Flow

4.5 Damping Effect by the Increase in Time-step

During initial tests for the wave model in the previous section, highly divergent free surface behaviour appeared and was magnified by the effect of waves when using small time steps of t = 0.005s. This was similar to the sink and trim analysis in still water of section 4.3 with a fine mesh using a time step of t = 0.005s. However when reverting to time steps of t = 0.01s the divergence behaviour was damped.

The method used for the computation was the Backwards Euler method. As a smaller time step is used the convergence of the result is more accurate but the stabilisation effect is reduced, this allows some diffusion of the results. By increasing the time steps damping is introduced to the iteration which reduces the effect of diffusion. Therefore a compromise must be found between achieving an acceptably accurate result whilst avoiding damping out any realistic behaviour of the free surface.

The fine mesh model was retested with an increased time step of t = 0.01s at the same range of Froude numbers.

Results Analysis

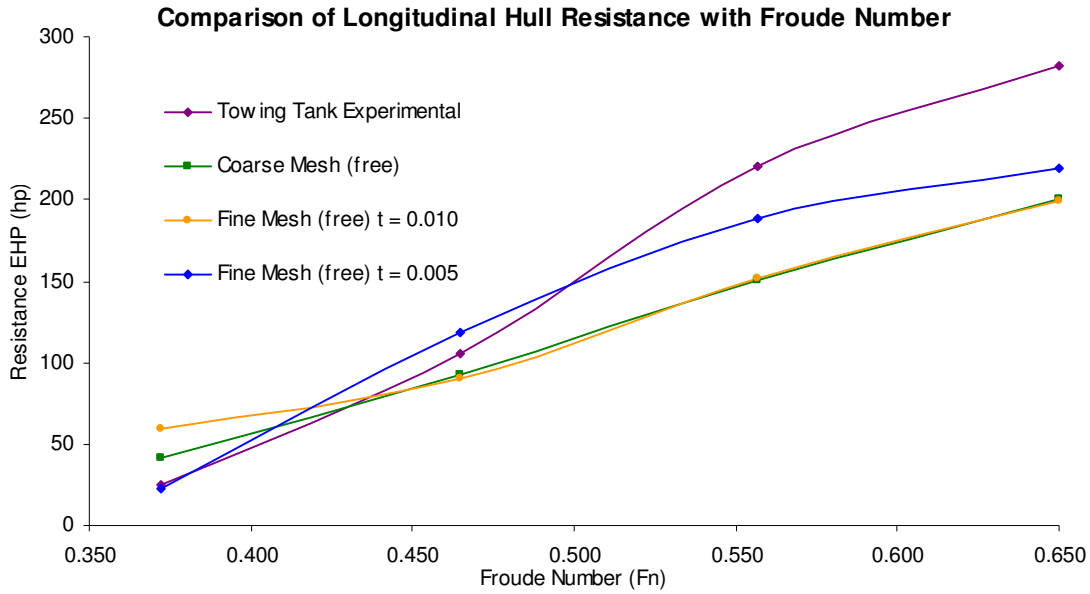

Figure: 4.19

Figure 4.18 compares data from the coarse mesh and the latest test with a fine mesh but increased time step. Surprisingly, this test produced results that were virtually identical to that of the coarse mesh. Also figures 4.19 and 4.20 shows the free surface of the fine mesh with the original and increased time steps respectively. It is clear in figure 4.20 that the diffusive nature of the free surface had disappeared and the bow wave looks much more similar to that of the coarse mesh.

This comparison shows that the increased time step reduces the accuracy of the results but damps out the diffusion of the free surface capture. This demonstrates that if both the fine and coarse mesh models use the same time step, they produce nearly identical results.

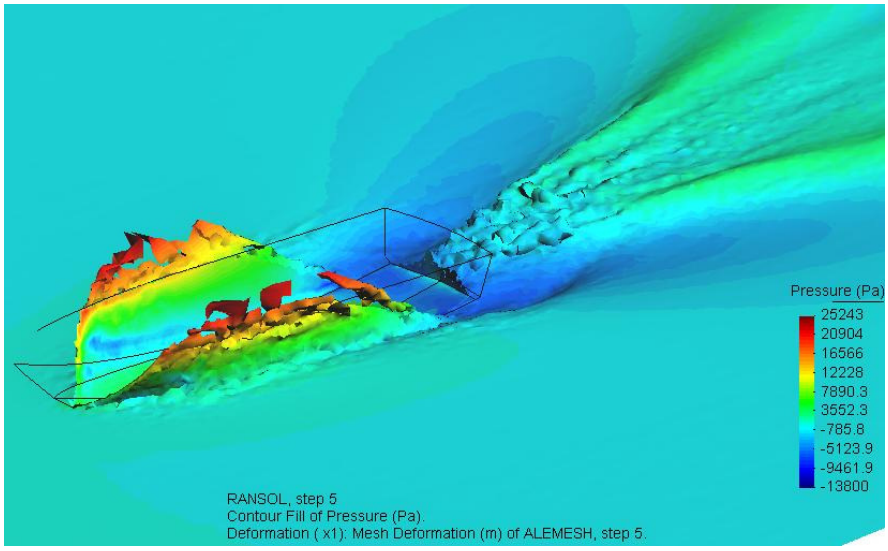

Figure: 4.20

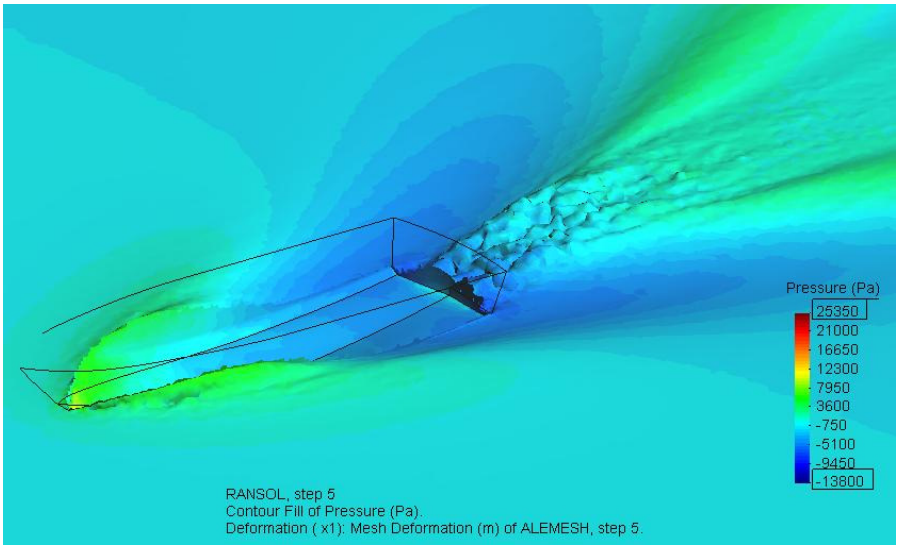

Figure: 4.21

4.6 Bi-Wigley Catamaran

As an extension to the project it was decided that a Catamaran hull would be tested using a model with the same configuration. The Catamaran in figure 4.21 and 4.22 has a Bi-Wigley hull configuration with a length, separation ratio of S/L = 0.3. The hull has an overall length of 10m, depth of 0.958m and a draft of 0.625m

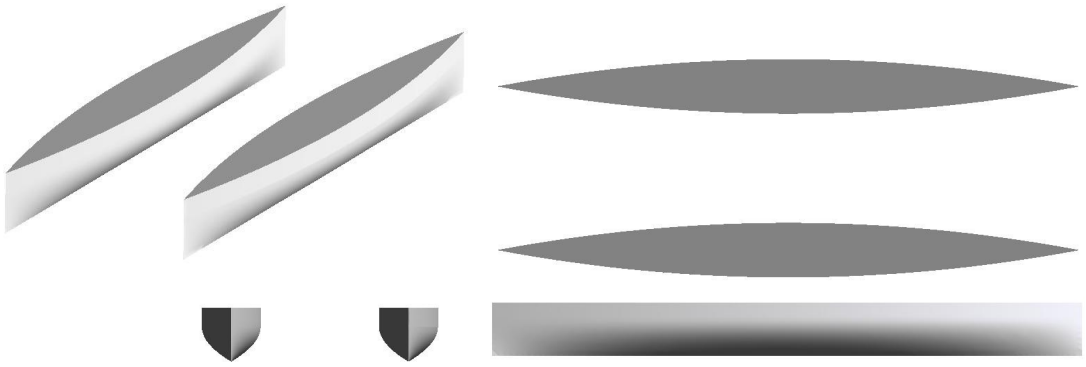

Figure 4.22: Isometric and three views of Bi-Wigley Catamaran.

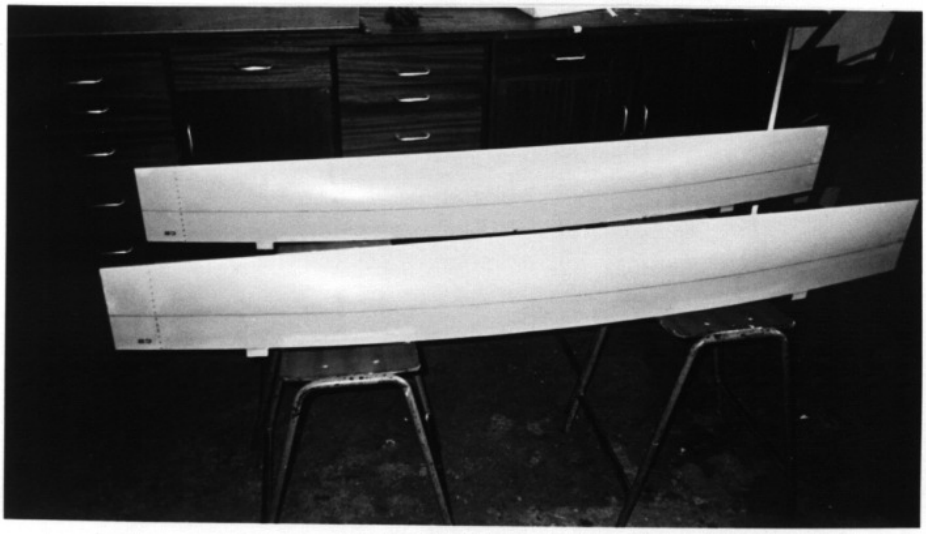

Figure 4.23: Photograph of Bi-Wigley Catamaran towing tank model [10]

4.6 Sink and Trim Analysis in Still Water

Tdyn Model Description

The model is configured in the same way as the NT-130 still water tests however the element size at the wave layer is 0.21m giving a mesh size of 1.9 million elements.

Results Analysis

The model was run for T = 9.0s and due to the small element size a time step of t = 0.005s was used. Appendix F figure F.1, shows longitudinal pressure force for the Fn = 0.4 test oscillating between the positive and negative regions and a divergent negative longitudinal pressure force in Fn = 0.2. The same results for Fn = 1.0, 0.8, and 0.6 were less erratic but are equally inconclusive. The longitudinal viscous forces in figure F.2 were as expected where the viscous force increased with Froude number, however a small amount of oscillation was present in the data.

The sink and trim data was highly oscillatory giving invalid results figures F.3 and F.4. Trend lines were added to the raw data to give some perspective of the possible sink and trim results convergence in figures 4.23 and 4.24. From conclusions drawn from section 4.5 it is possible that the small time step could have caused some dispersion in the results.

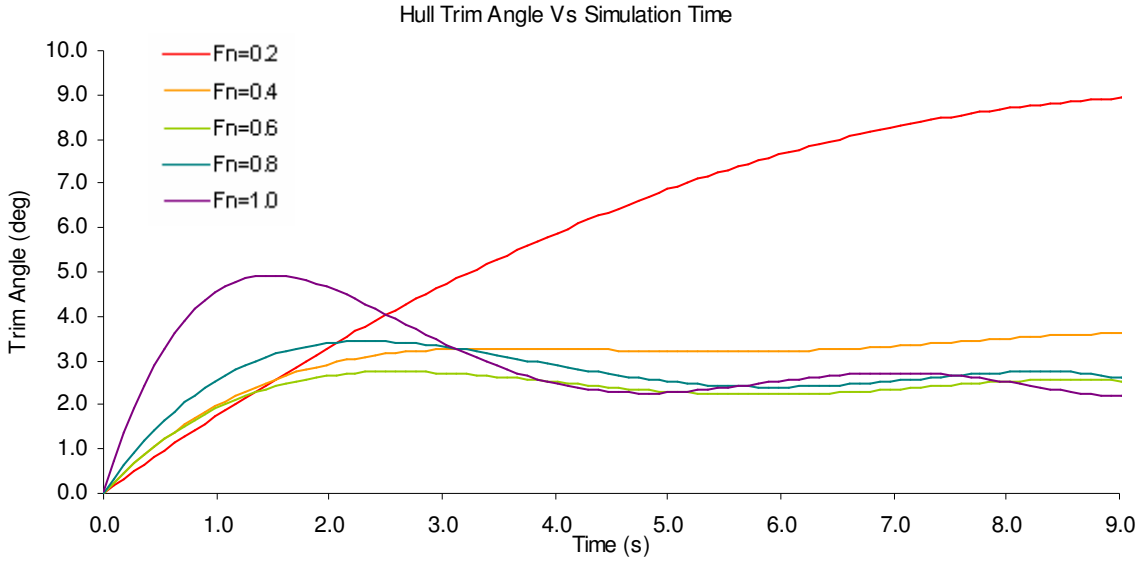

Figure: 4.24

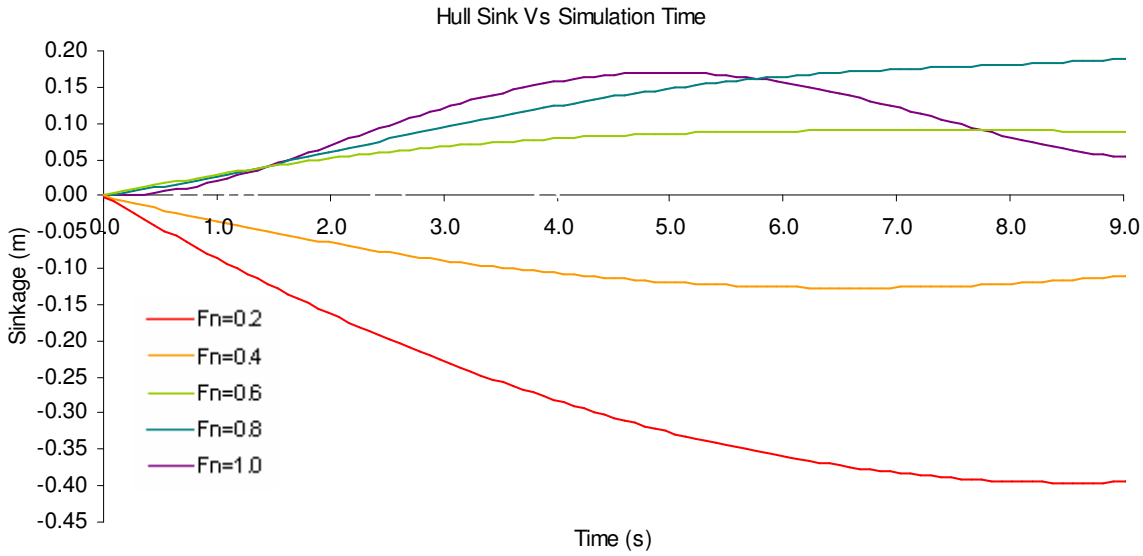

Figure: 4.25

The following figures 4.25 and 4.26 shows the sink & trim, free surface deformation and dynamic pressure distribution for the Fn = 1.0 test. The computation with this Froude number was chosen because it showed the least divergent and unstable behavior in its results. Figure 4.26 shows the development of a wake in a plan view for a Catamaran over a period of 9 seconds. The area of negative pressure in blue can be seen receding aft of the hull and stabilizing in the troughs of the wake. Also the pattern of interaction between the wakes from the two hulls can be clearly identified. The contact of the inner crests of the bow waves can be seen creating an area of high pressure between the hulls. This in turn creates an trough of negative pressure half a hull length behind the stern and another area of high pressure 1.5 hull lengths behind the stern.

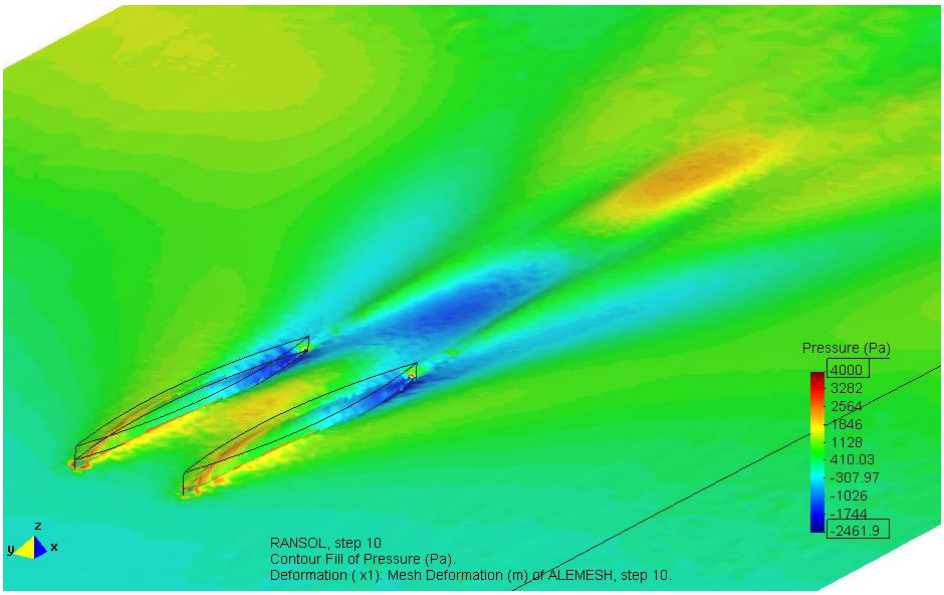

Figure 4.26: Isometric view of flow visualisation for Catamaran wake development.

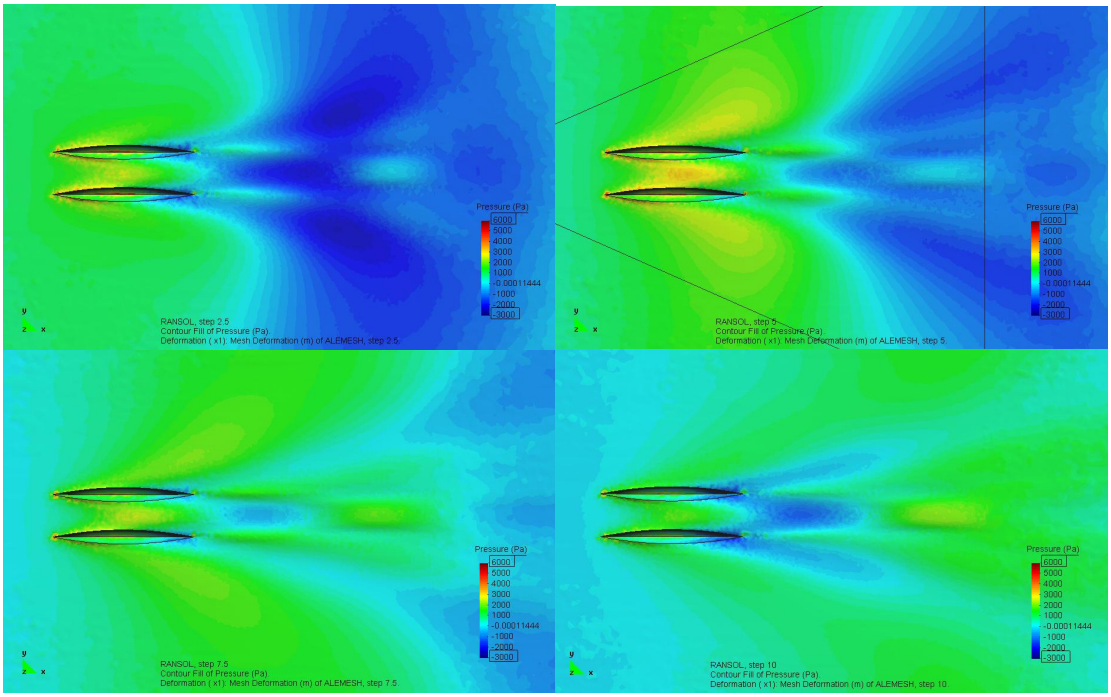

Figure 4.27: Plan view of flow visualisation for Catamaran wake development.

5.0 Conclusion

Overall, Tdyn performed well in the simulation of the NT-130 hull producing accurate result in comparison to experimental towing tank data. The longitudinal resistance data from tests in still water conditions with a fine mesh were particularly outstanding with low percentage errors. Although some anomalies were found regarding the free surface capture of this example, development of this software has already begun to solve these problems.

The first series of tests involved running the model with range of different CG positions to simulate the effect of adverse locating configurations. This uncovered some interesting behaviour of the hull. The reference point taken at the most forward point of the waterline and CG were measured in meters aft of this position. As the CG was located at the most forward position 5.0m, the boat was found to have a negative trim even at full speed (14kts, Fn = 0.65) with an increased longitudinal resistance. This condition should be avoided to minimise drag on the hull. As the CG was shifted to its opposite extreme 8.0m, the hull was found to trim at over 8 degrees but with a significantly reduced resistance. This condition should also be avoided as the forward vision of the crew would be obstructed. Also, at such a high angle of trim the lateral stability of the hull would be greatly reduced with the length of the waterline.

The focus of this project is with the main series of tests involving the NT-130 hull in still water conditions. This model was run with the configurations: Fixed hull, free to sink and trim for a coarse and fine mesh. The computations with a fixed hull were to initially test if ODDLS could produce satisfactory surface capture for the bow wave and wake, with a relatively short computation time. As expected this produced longitudinal resistance that was quite inaccurate and turned out to be very similar to the previous CFD method. Once this model was given freedom to sink and trim, extra ALEMESH conditions were required to allow the mesh to deform in the vertical direction and rotate about the lateral axis. This dramatically increased the computation time from 6hrs to 10hrs. The results did not show any more correlation to the behaviour of experimental data but a quantitative increase over the whole range of Froude numbers.

Finally, computations with a fine mesh and a hull free to sink and trim produced resistances with errors of only 10% to 22% from experimental results, very good for this type of analysis. However, when post processing the data for these tests, the free surface capture was found to have some unexpected bow wave behaviour. The crest of the bow wave was found to rise above the freeboard of the hull and extending to almost the length of the waterline. Later tests determined it to be a problem of dispersion in the backwards Euler scheme. As the time step was reduced so was the accuracy of the converged results, however this applied a level of stabilisation and damped out any dispersion in the free surface capture. We have yet to determine the nature of these high bow waves and whether if reducing the time step would damp out any realistic effects.

The original model was adapted to run with waves and computations produced promising results. Many features of a hull travelling through wave conditions were captures on the free surface. Data has been included in the validation and appendix of this project including several animations in the DVD to further analysis.

Tests with the Bi-Wigley Catamaran model proved inconclusive and produce results that were unexpected and random. With more time, an investigation into these results and modifications to the model could produce some comparative results to towing tanks experiments.

6.0 Further Work

Due to the time restrictions of this project many areas of this project has scope for improvement and development:

- Obtaining thrust vector and towing moment of NT-130 from Navtec, development of the model can include these components and further improve the accuracy of these results. As the hull sink and trim during acceleration, the thrust vector would also change causing pitching moments on the hull.

- An investigation can be made to find the optimum time step for fine mesh computations to find a balance between the damping and accuracy of convergence for the results Furthermore, with more time a finer mesh with over 10million elements can be produced further improving the accuracy.

- Diagonal waves can be applied to the model with changes to the assignment of boundary conditions. The behaviour of lateral pitch characteristics can uncover any capsizing behaviour of this hull.

Professor Garcia has already begun making improvements to the Tdyn code that will be included in the next release including:

- Advanced scheme for nodal assembling of the advective and diffusive terms.
- New reinitialisation algorithm for level set equation.
- Improved 4th order stabilisation scheme for advection (Auto option).
- Improved ILES turbulence model.
- Improved ALE stabilisation scheme.

An example of this work can be seen in figure 6.1 below, where the model was run with 14m million elements. With the changes includes a 30% reduction in computation time for this type of analysis.

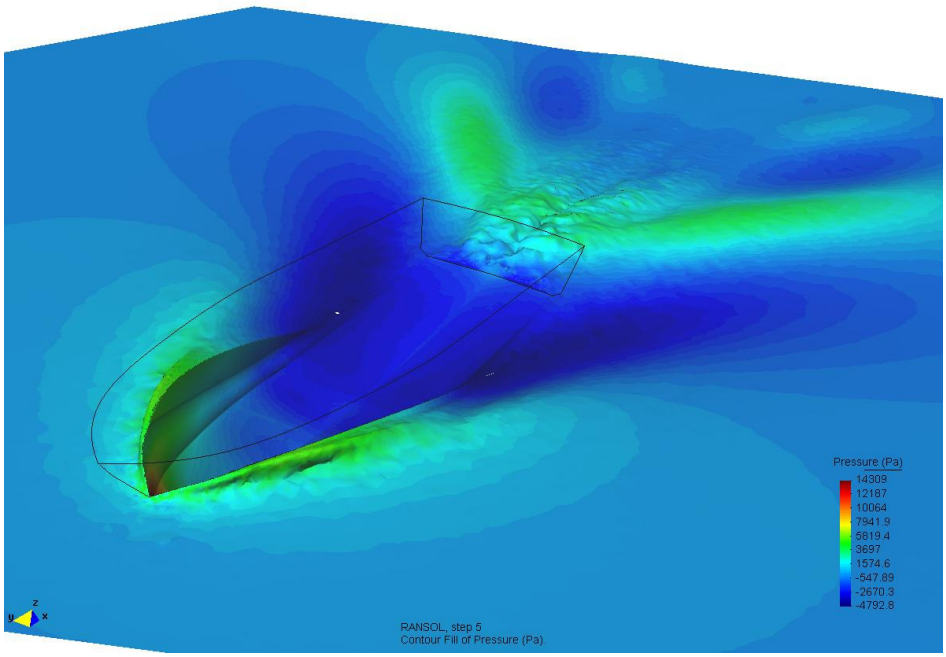

Figure 6.1: Flow visualization with improved Tdyn code
(Courtesy of Prof Garcia, Compass Ingeniería y Systemas)

References

[1] E. Oñate, J. García, “A finite element method for fluid-structure interaction with surface waves using a finite calculus formulation”, Computer methods in applied mechanics and engineering, Vol. 191, 635–660. (2001)

[2] J. García, E. Oñate, “An Unstructured Finite Element Solver for Ship Hydrodynamics Problems”, Journal of Applied Mechanics, Vol 70, 18-26. (2003)

[3] E. Oñate, J. García, S.R Idelsohn, F. Del Pin, “Finite Calculus Formulations for Finite Element Analysis of Incompressible Flows. Eulerian, ALE and Lagrangian Approaches”, Computer methods in applied mechanics and engineering, 3001–3037. (2001)

[4] R.A. Royce, “A Rational Prismatic Hull Approach for Planning Hull Analysis”, Society of Naval Architects and Marine Engineers.

[5] J. García, A. Valls, E. Oñate, “ODDLS: A New Unstructured Mesh Finite Element Method for the Analysis of Free Surface Problems”, Compass Ingeniería y Systemas, International Centre for Numerical Methods in Engineering (CIMNE).

[6] S. Osher, R.P Fedkiw, “Level Set Methods: An Overview and Some Recent Results”, Journal of Computational Physics, Vol 169, 463–502 (2000)

[7] J. García, A. Valls, E. Oñate, “Perspectives of the Finite Increment Calculus Method in the Numerical Modeling of Turbulence for Naval Problems”.

[8] R. Codina, J. Principe, O. Guasch, S. Badia, “Time Dependent Subscales in the Stabilized Finite Element Approximation of Incompressible Flow Problems”.

[9] E. Oñate, A. Valls, J. García, “FIC/FEM Formulation with Matrix Stabilizing Terms for Incompressible Flows at Low and High Reynolds Numbers”, Computational Mechanics. (2006)

[10] M. Insel, “An Investigation into the Resistance Components of High Speed Displacement Catamarans”, University of Southampton, Ph.D Thesis. (1990)

[11] M. Insel, A.F. Molland, “An Investigation into the Resistance Components of High Speed Displacement Catamarans”, Transactions of Royal Institution of Naval Architects, Vol 133. (1992)

[12] J. Yang, “Time Domain, Nonlinear Theories on Ship Motions”, The Department of Ocean and Resources Engineering, University of Hawaii. (2004)

[13] L. Alvarez, F. Guichard, P.L. Lions, and J.M. Morel, “Axioms and fundamental equations of image processing” Arch. Ration. Mech. Anal. 123, 199. (1993)

Websites:
[14] GiD pre/post processor software webpage. “http://gic.cimne.upc.es”
[15] Tdyn computation software webpage. “http://www.compassis.com”
[16] J. A Sethian (1999) webpage. “http://math.berkeley.edu/ sethian”
[17] Semi-displacement hull definition webpage. “http://powerboat.about.com”
[18] Hull design webpage. “www.ellisboat.com/hullDesign”
[19] Naval architecture webpage. “http://en.wikipedia.org/wiki/Hull_(watercraft)”

Appendix A

Offshore Patrol Vessel NT-130: Investigation into the Effect of the Centre of Gravity Location

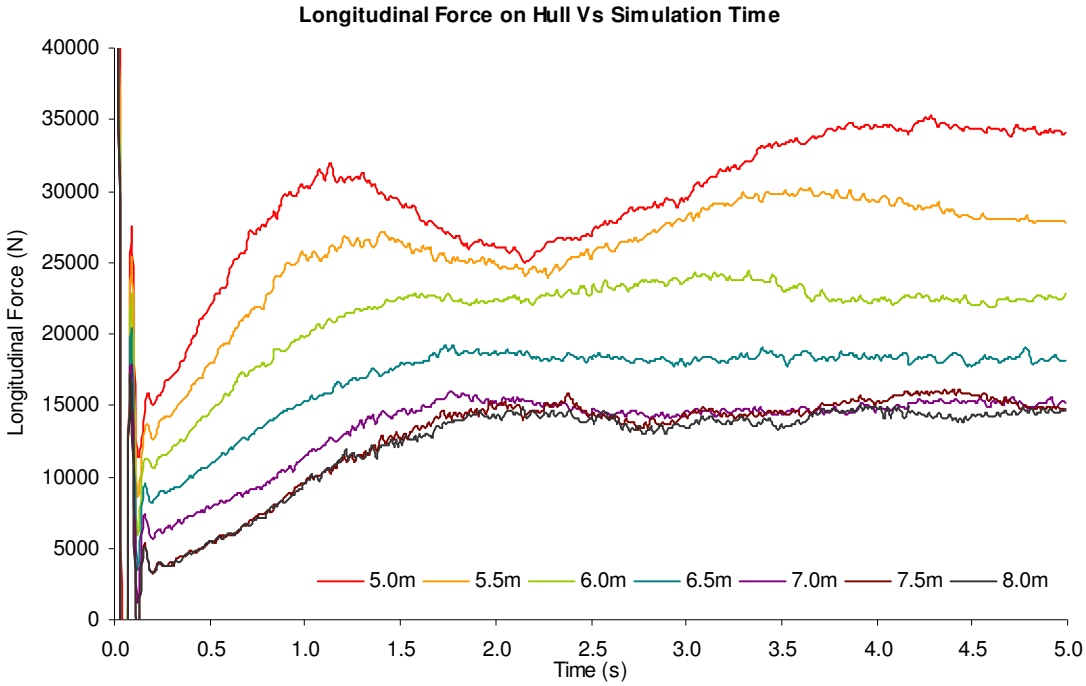

Figure: A.1

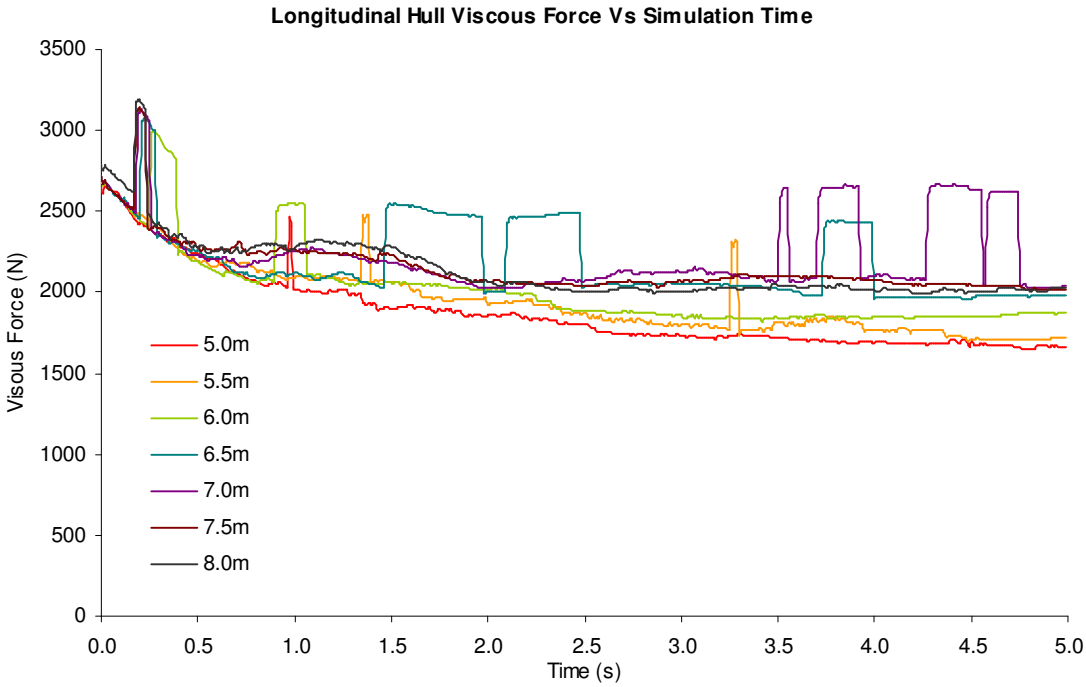

Figure: A.2

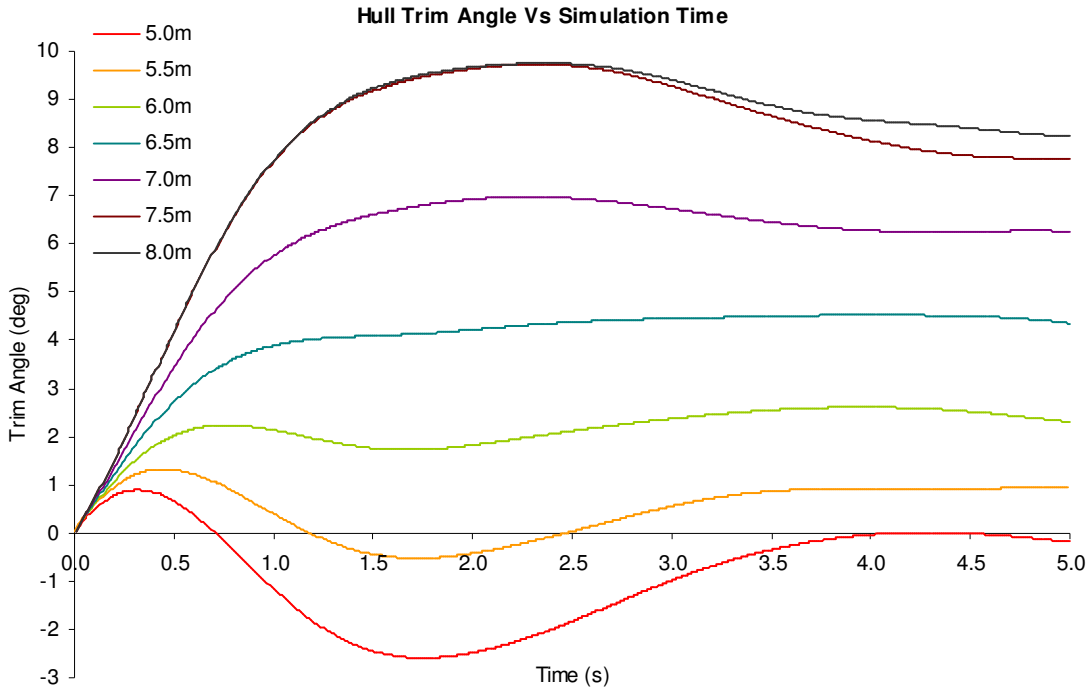

Figure: A.3

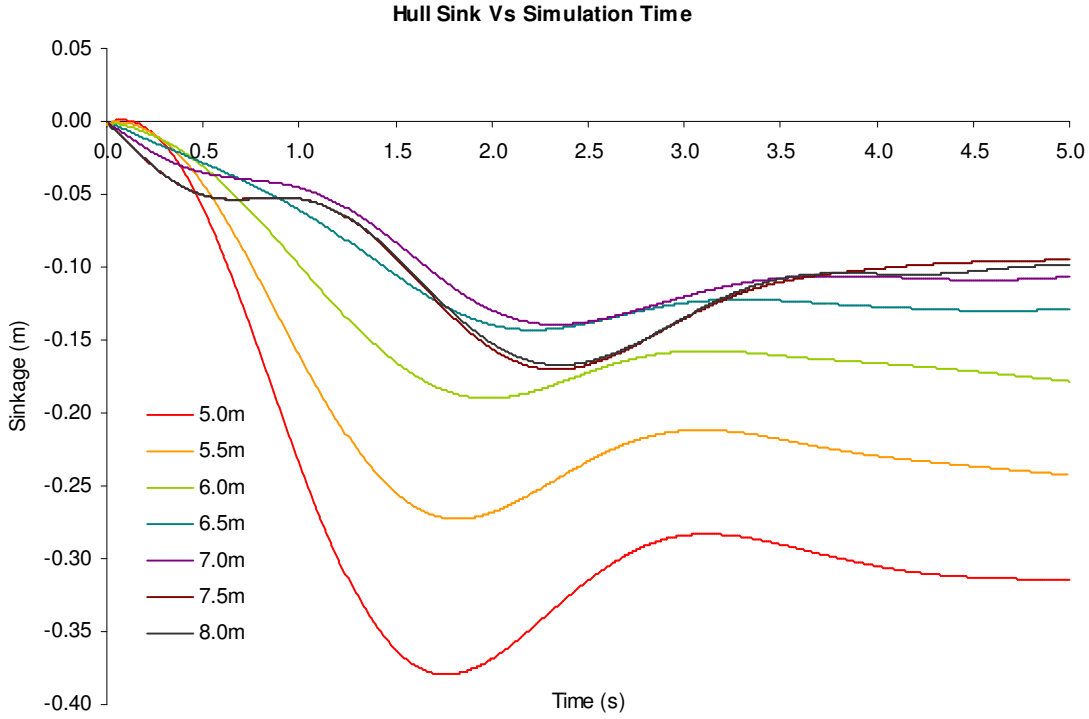

Figure: A.4

Appendix B

Offshore Patrol Vessel NT-130: Fixed Hull Analysis in Still Water

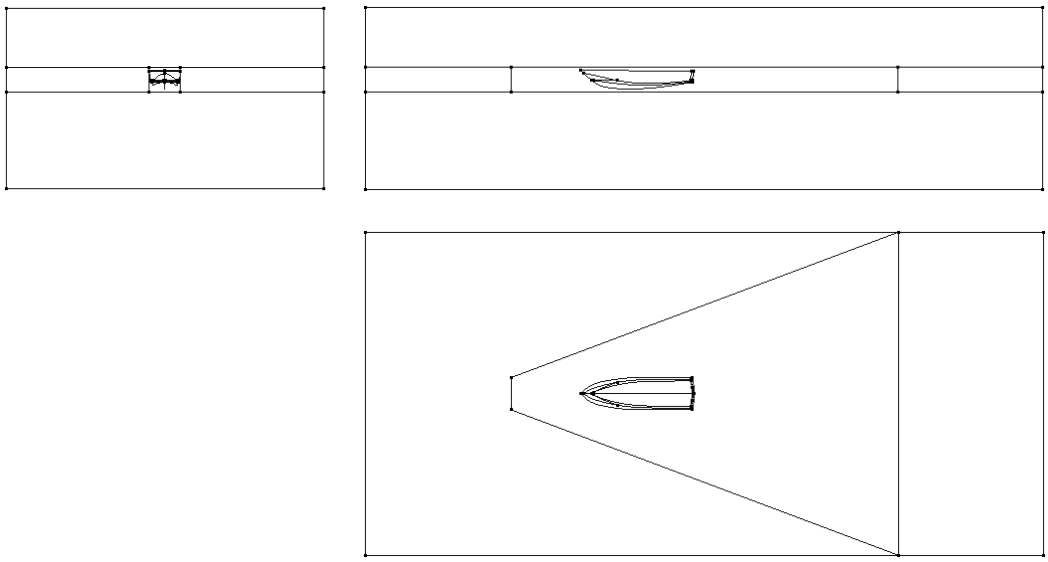

Figure: B.1

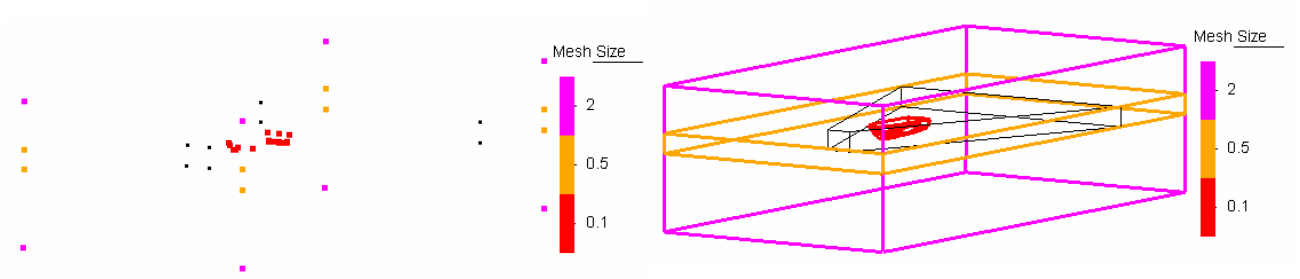

Point element size (m)

Line element size (m)

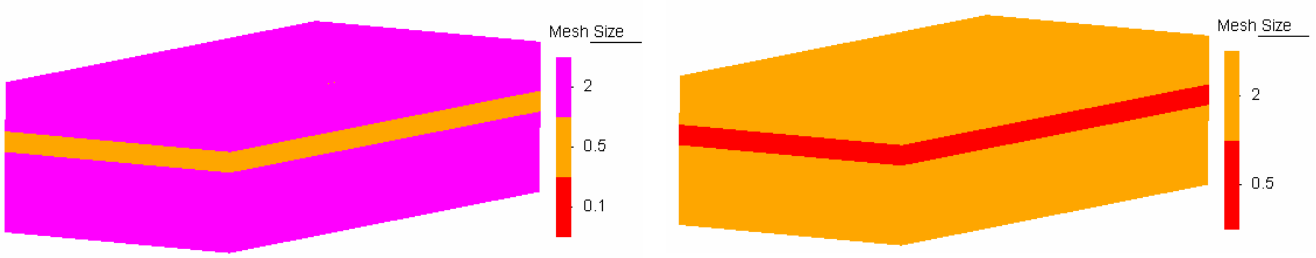

Surface element size (m)

Volume element size (m)

Figure: B.2

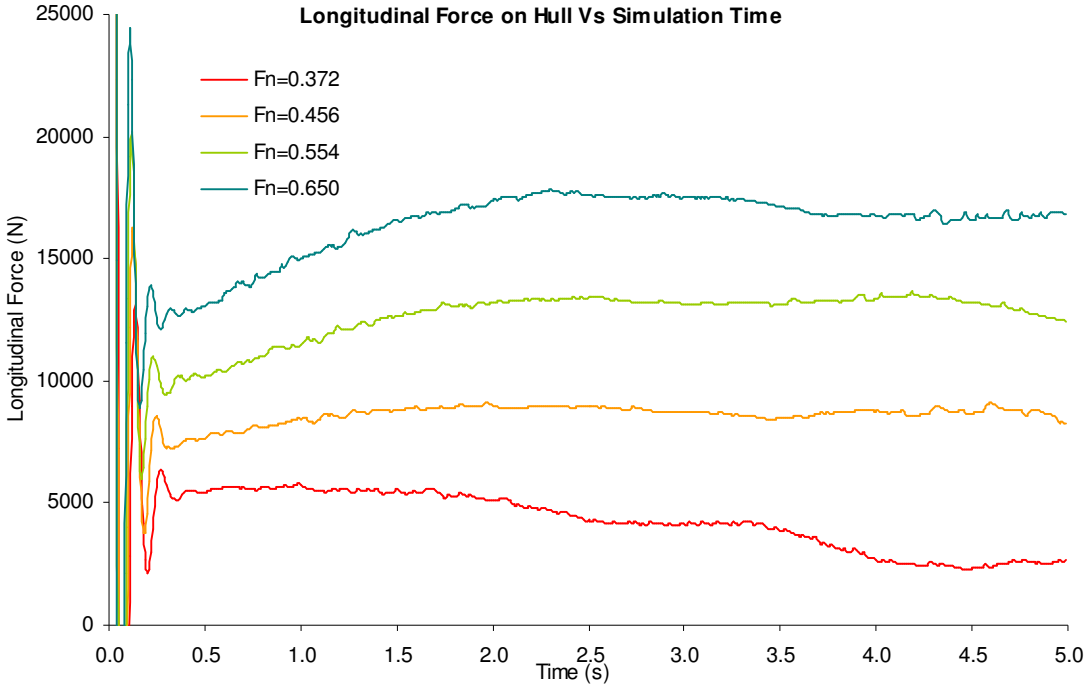

Figure: B.3

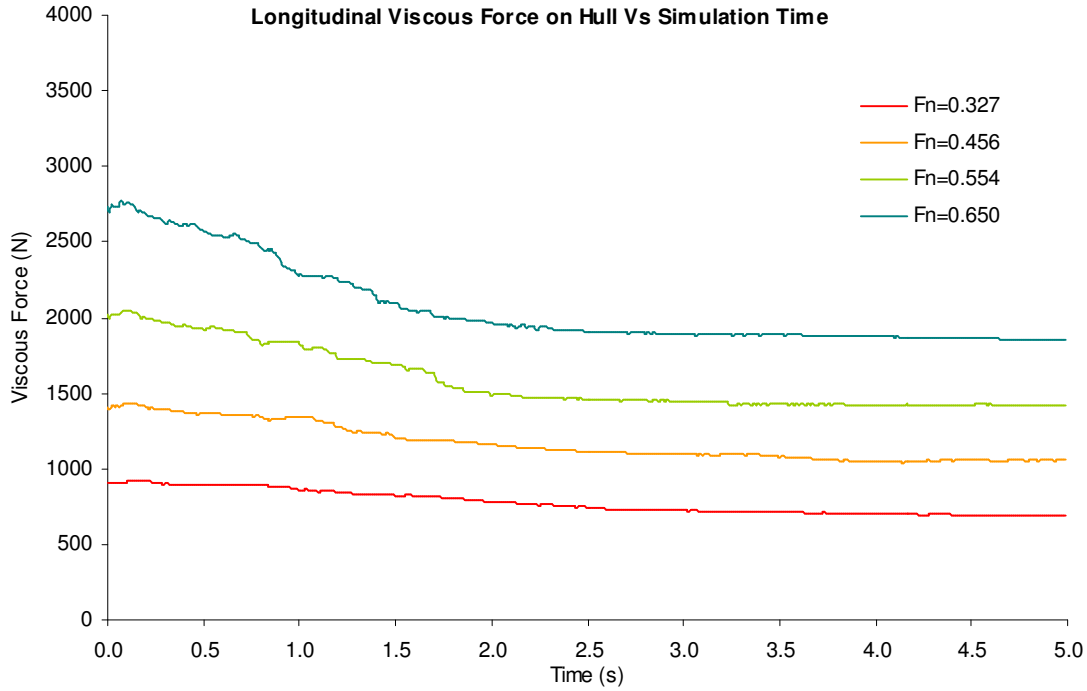

Figure: B.4

Appendix C

Offshore Patrol Vessel NT-130: Sink and Trim Analysis in Still Water

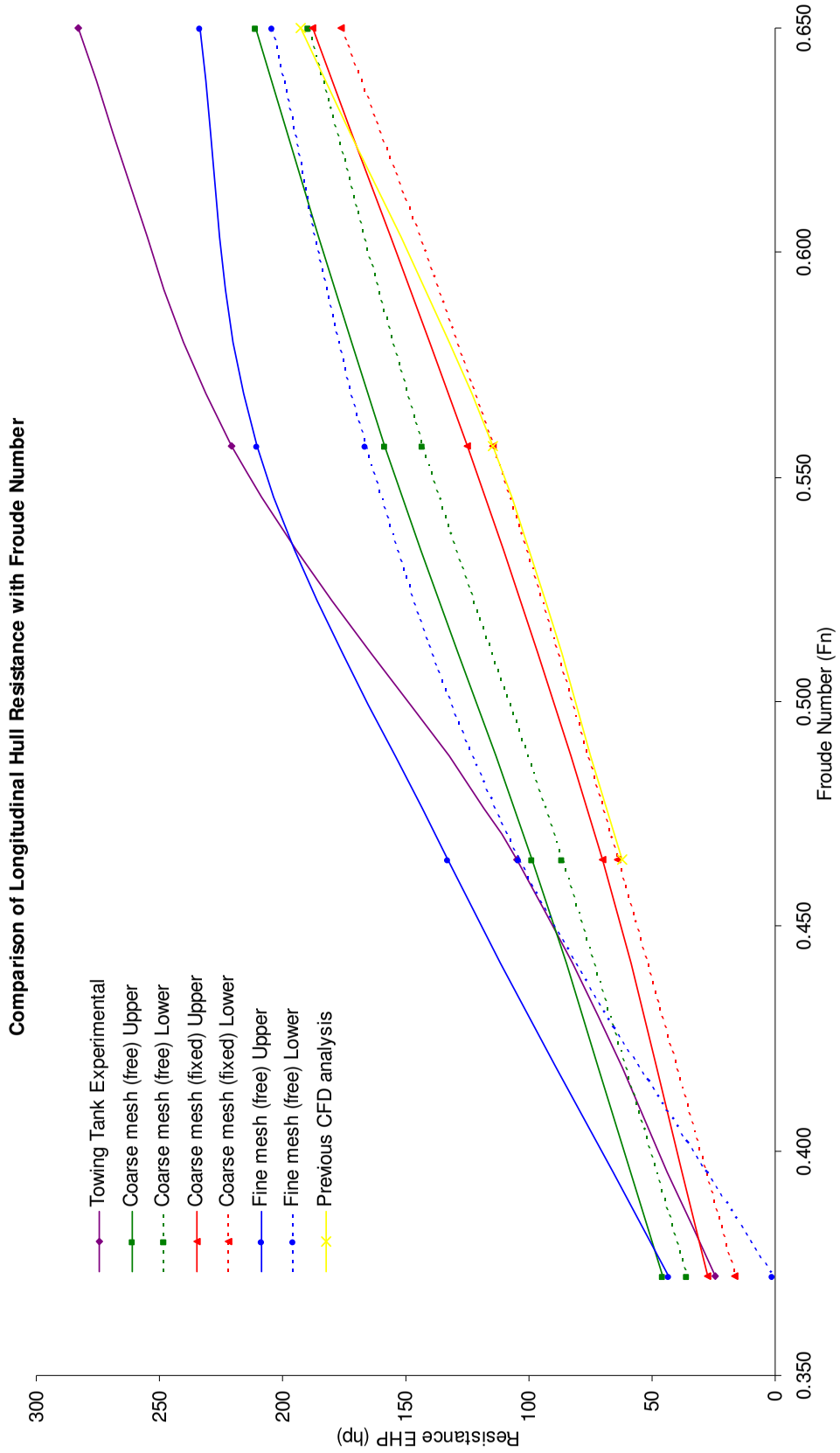

Figure: C1

Coarse Mesh Data

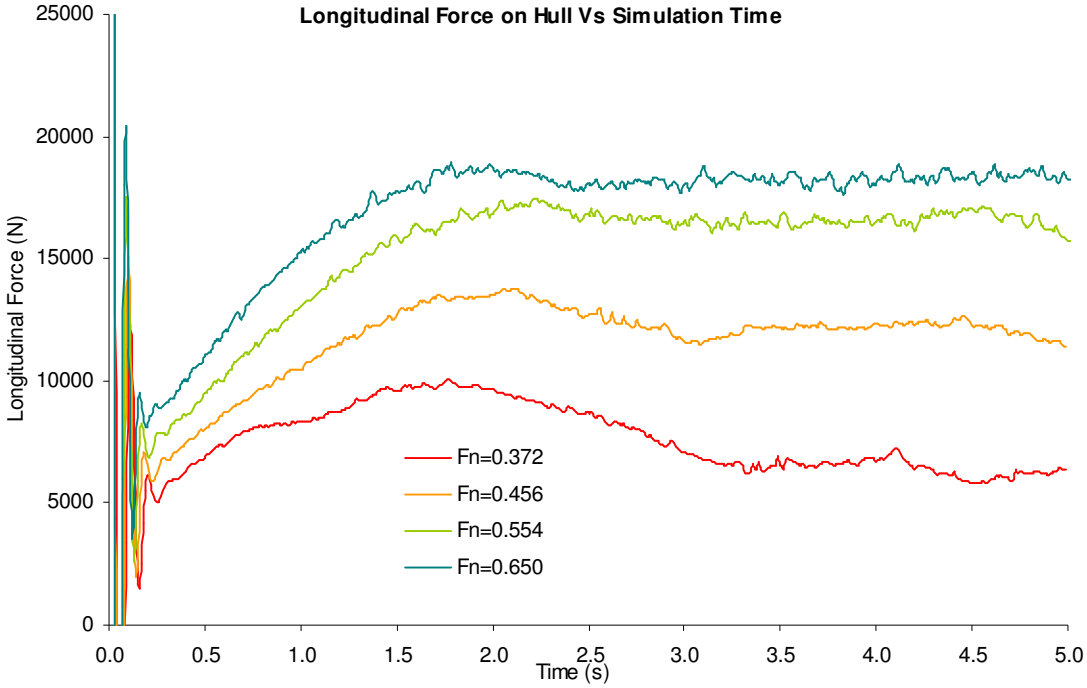

Figure: C.2

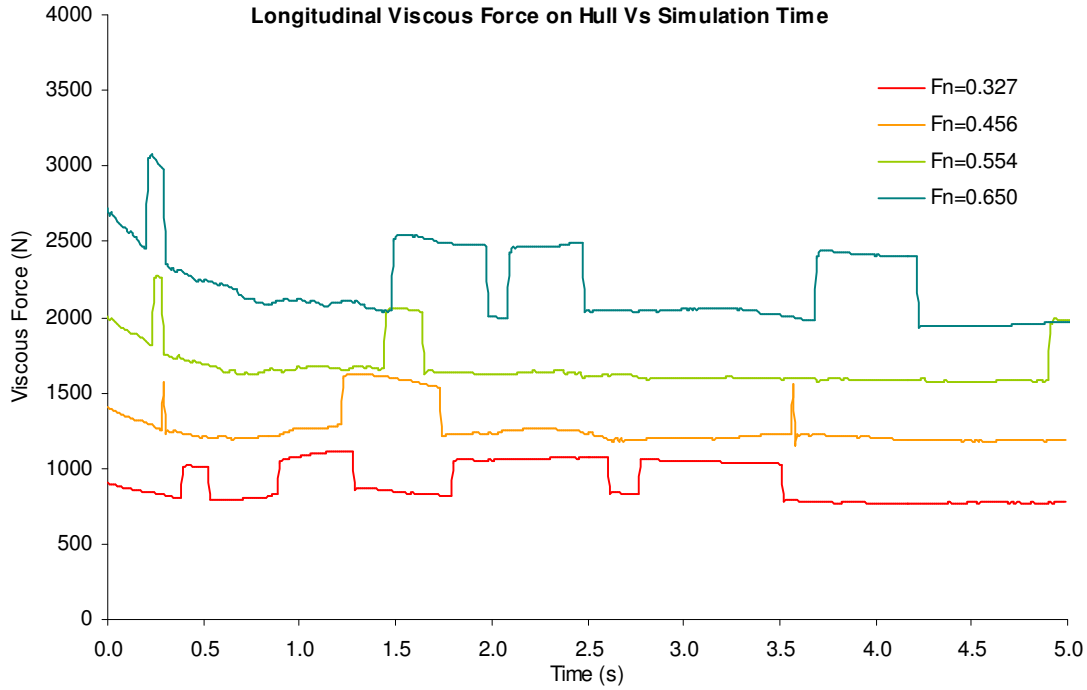

Figure: C3

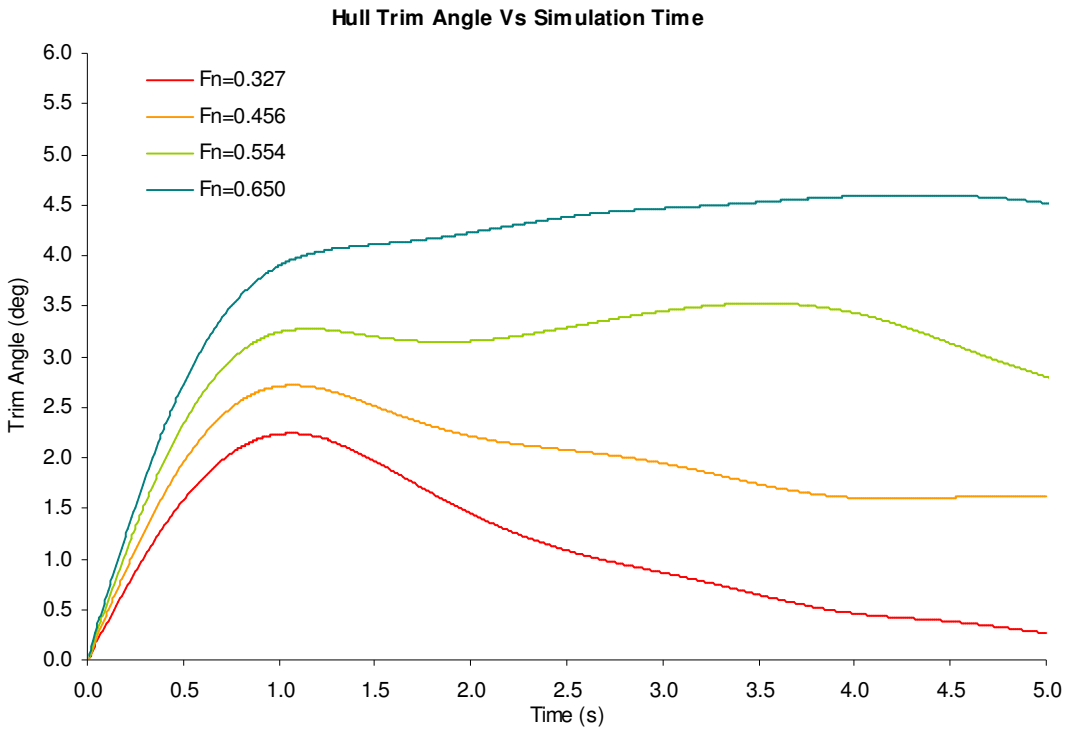

Figure: C.4

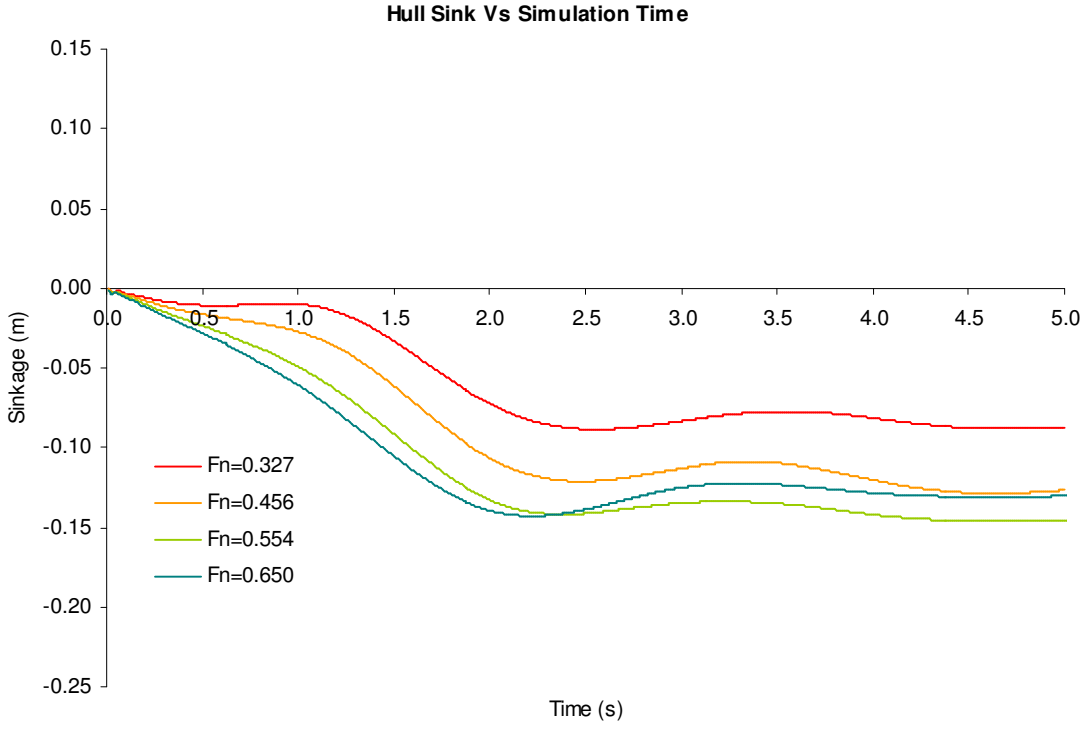

Figure: C.5

Fine Mesh Data

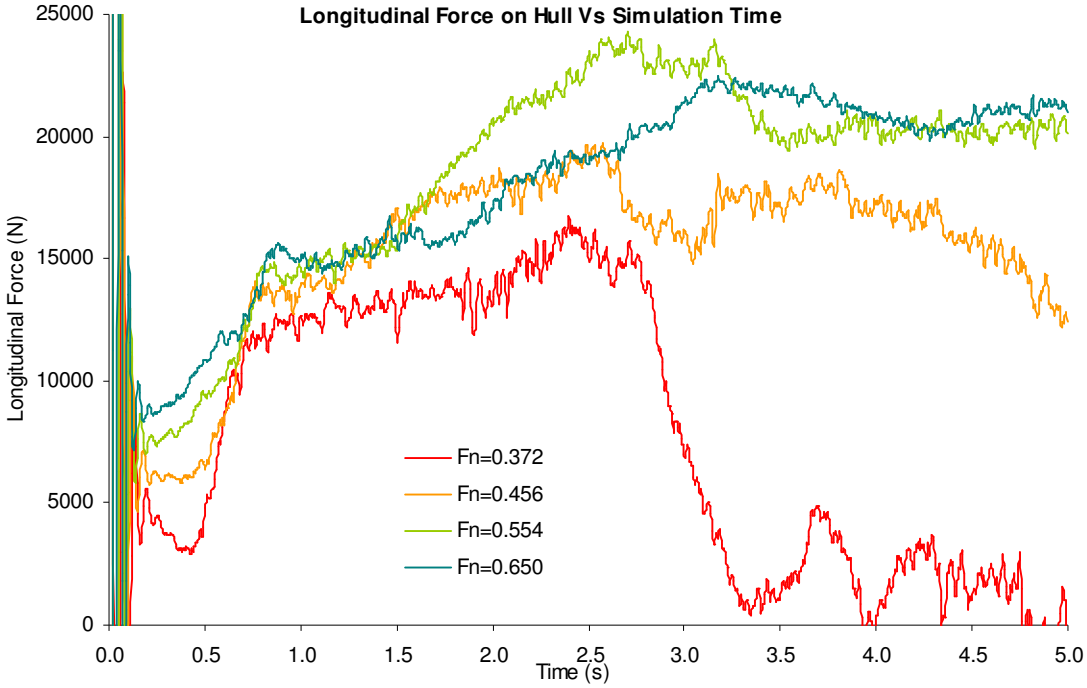

Figure: C.6

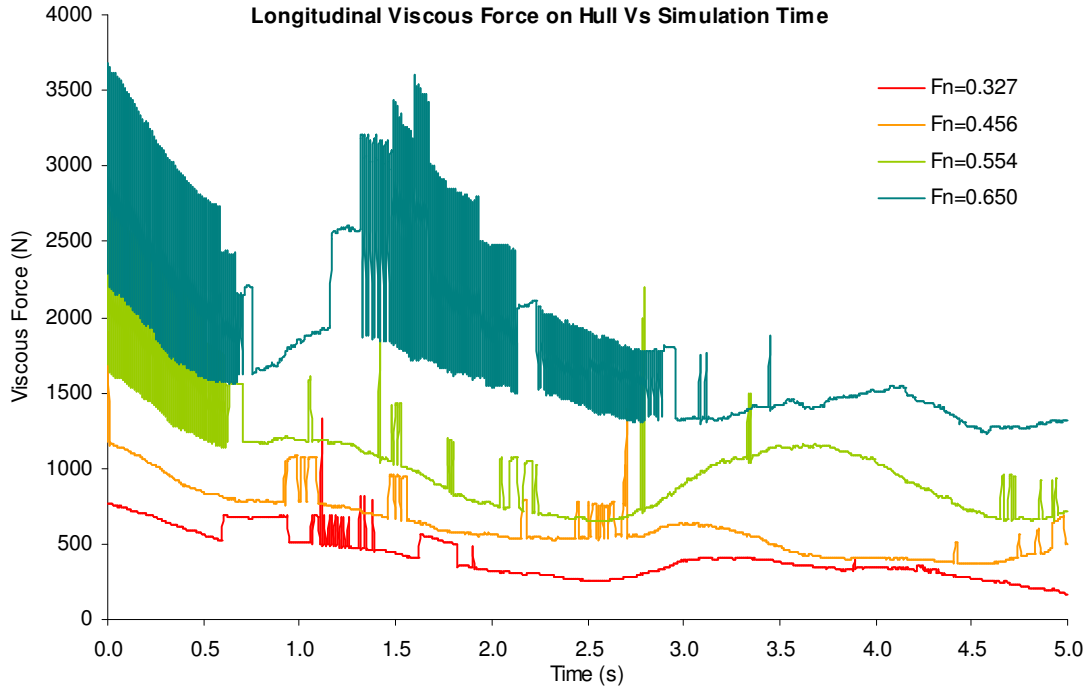

Figure: C.7

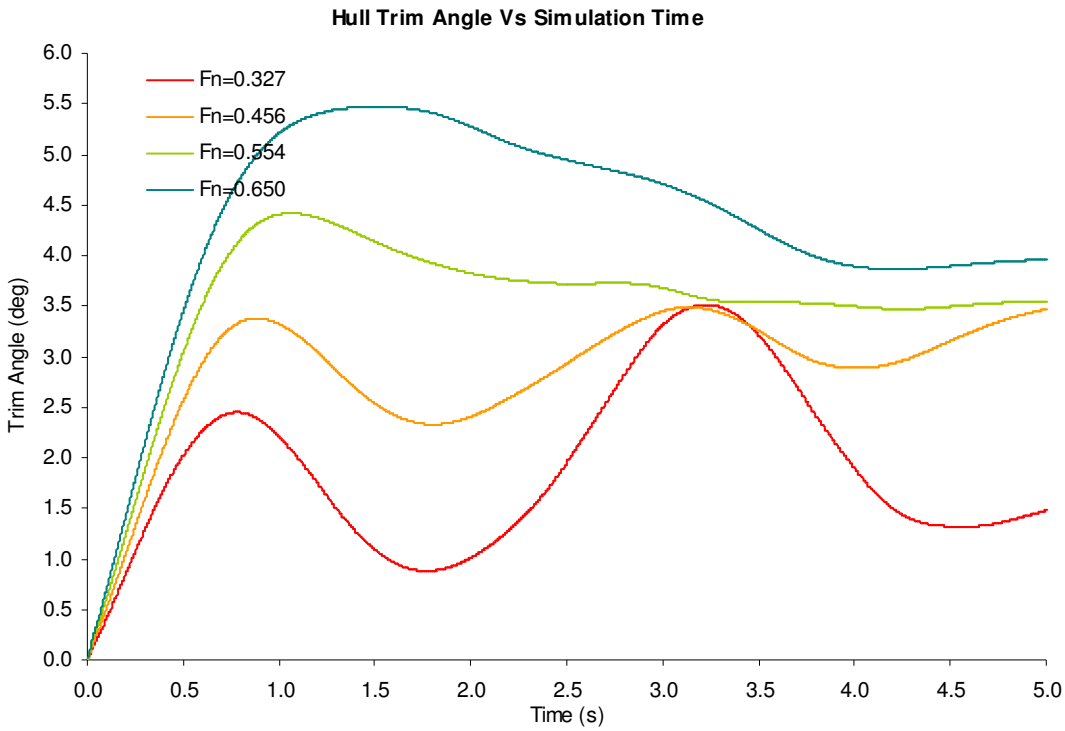

Figure: C.8

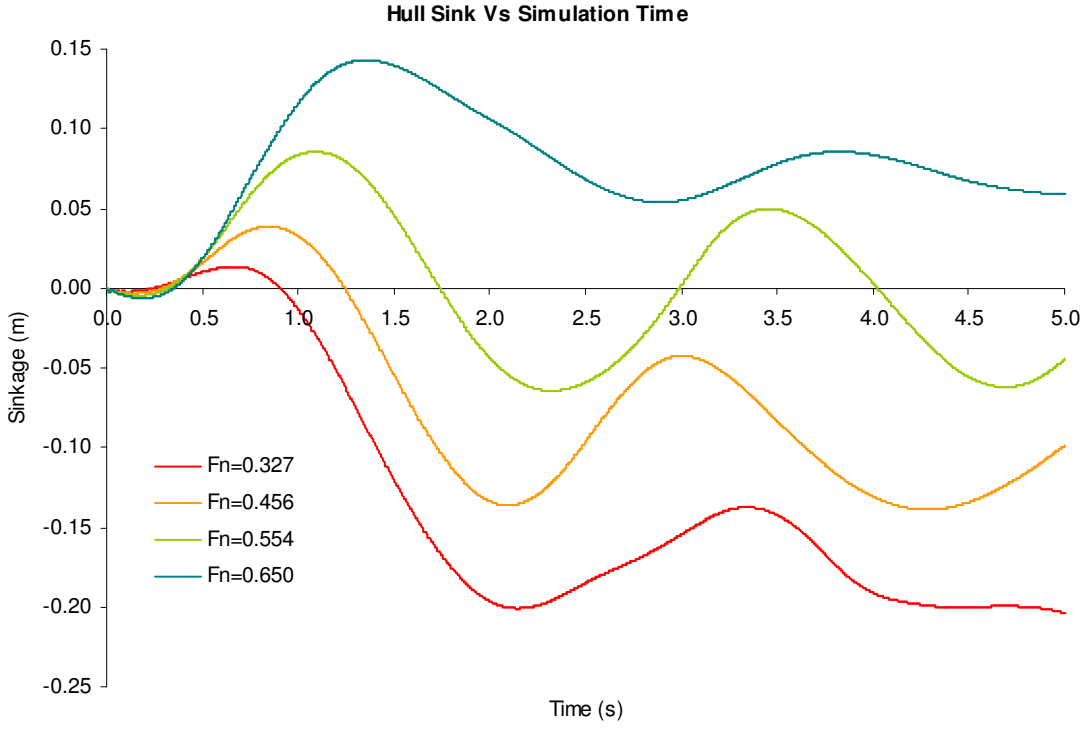

Figure: C.9

Appendix D

Offshore Patrol Vessel NT-130: Slamming Analysis in Waves

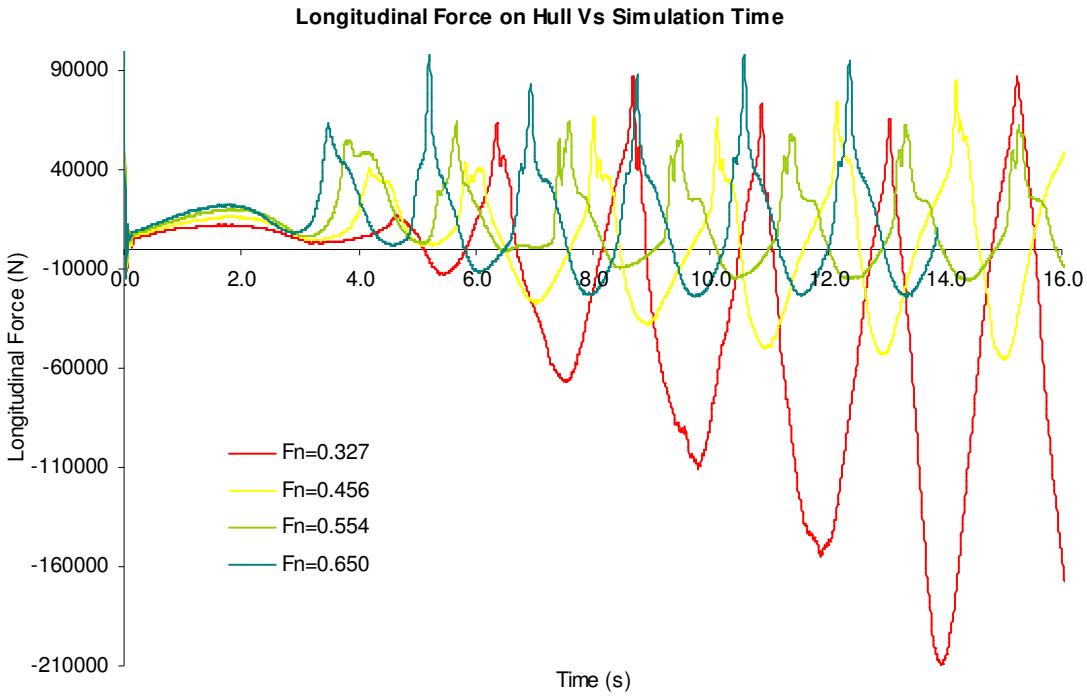

Figure: D.1

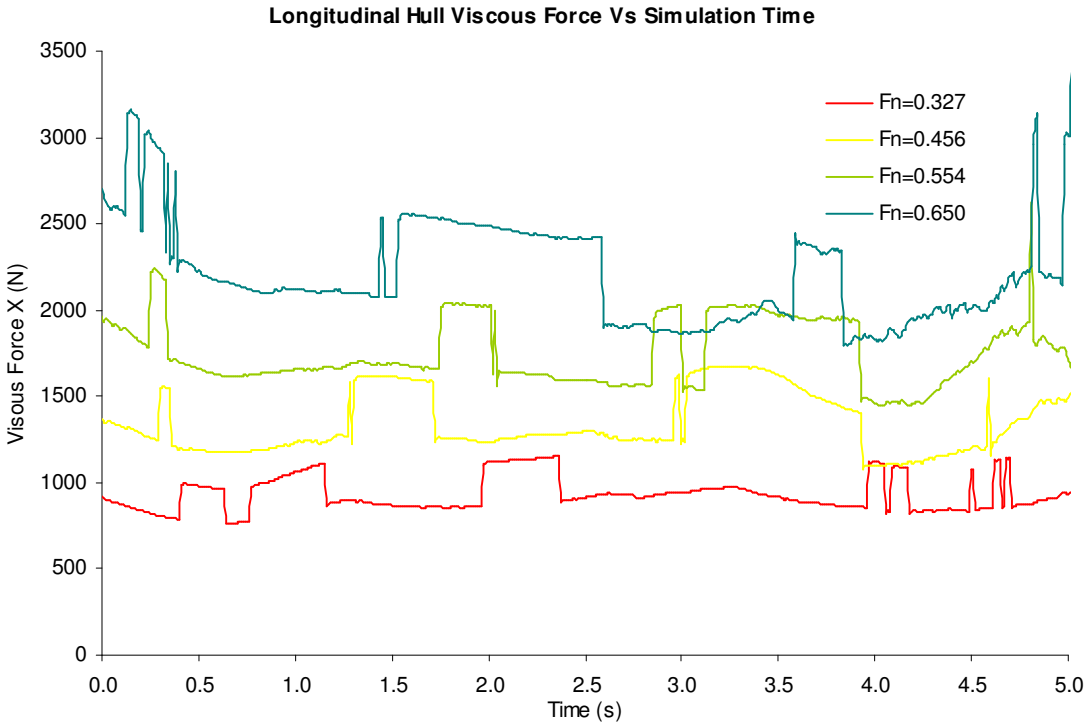

Figure: D.2

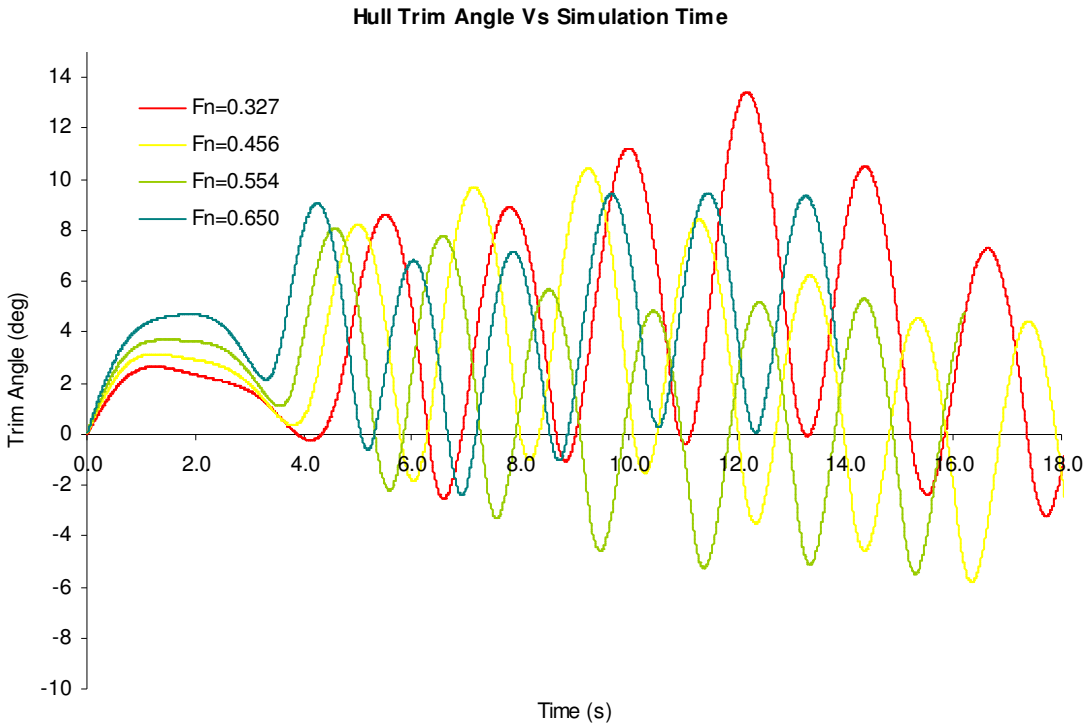

Figure: D.3

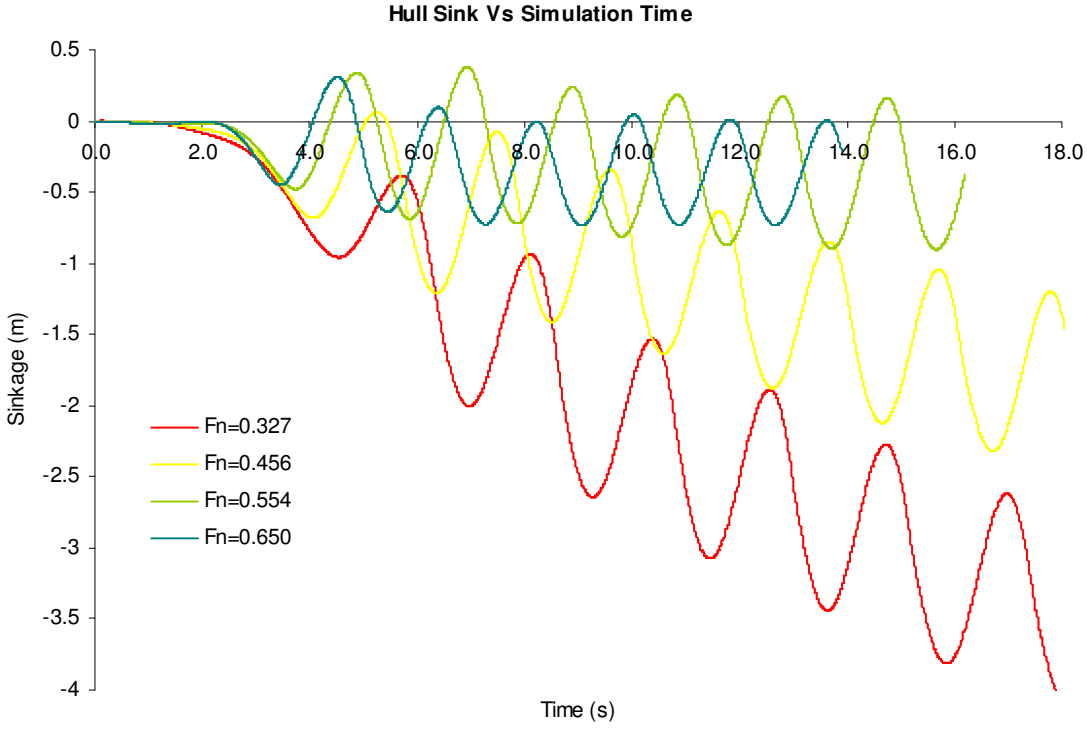

Figure: D.4

Divergent Case Fn = 2.0

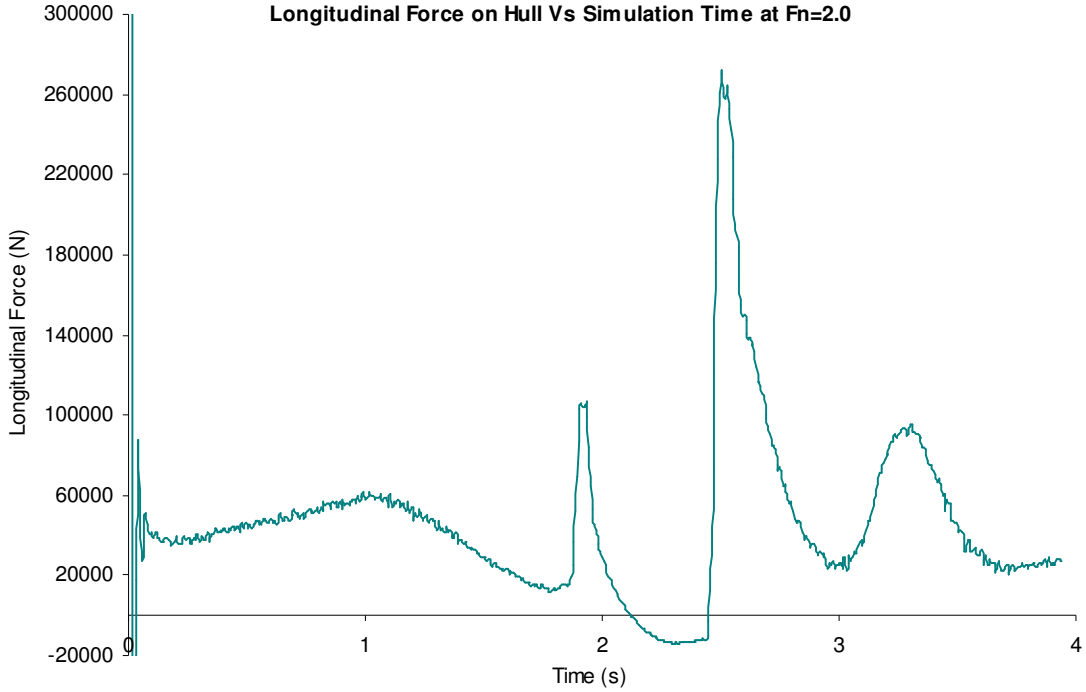

Figure: D.5

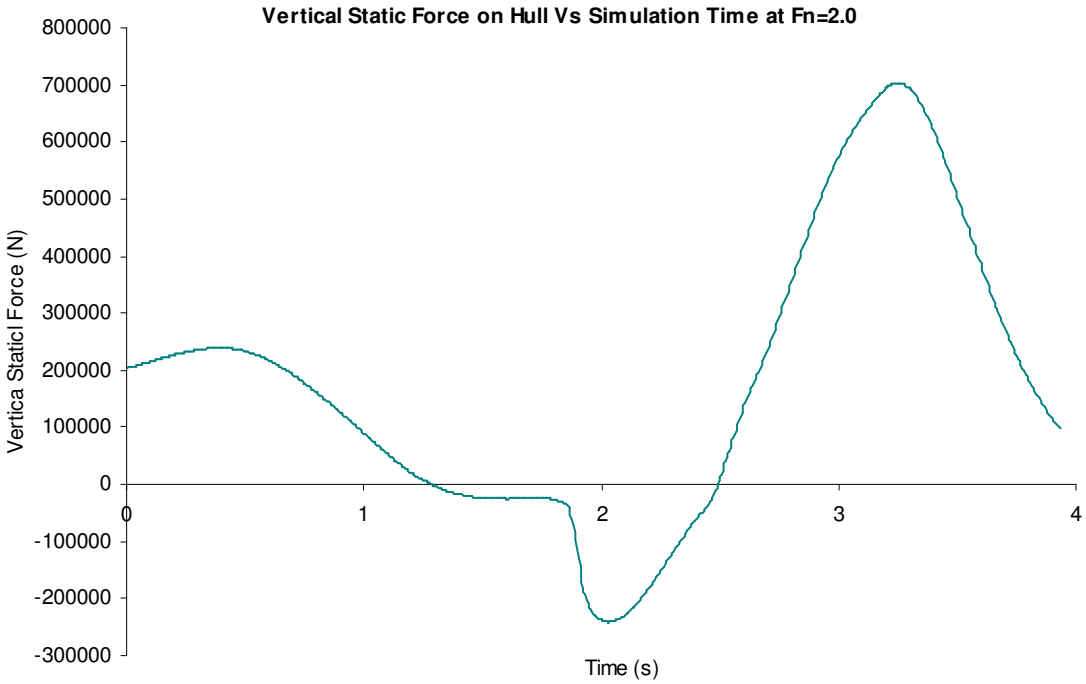

Figure: D.6

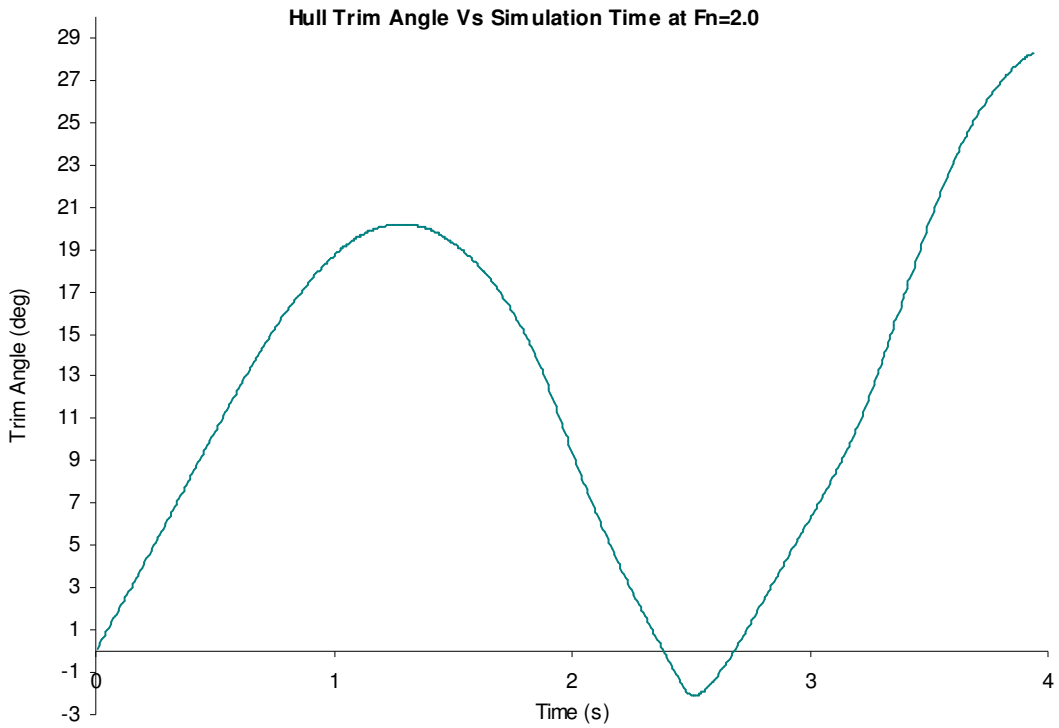

Figure: D.7

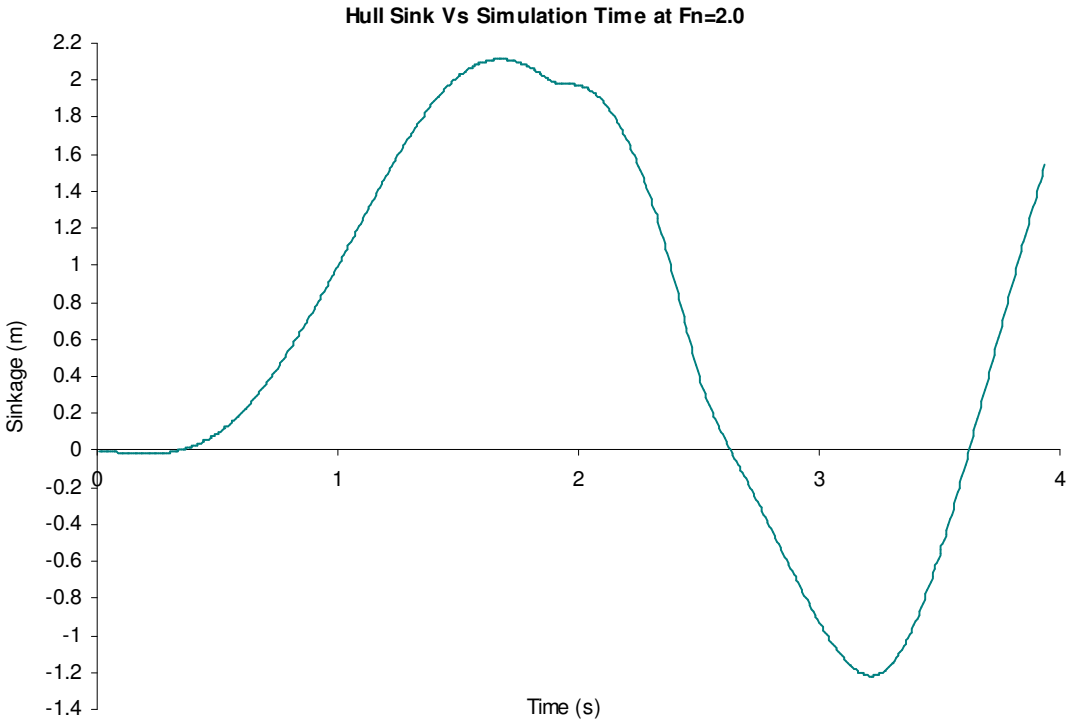

Figure: D.8

Appendix E

Offshore Patrol Vessel NT-130: Slamming Analysis in Waves

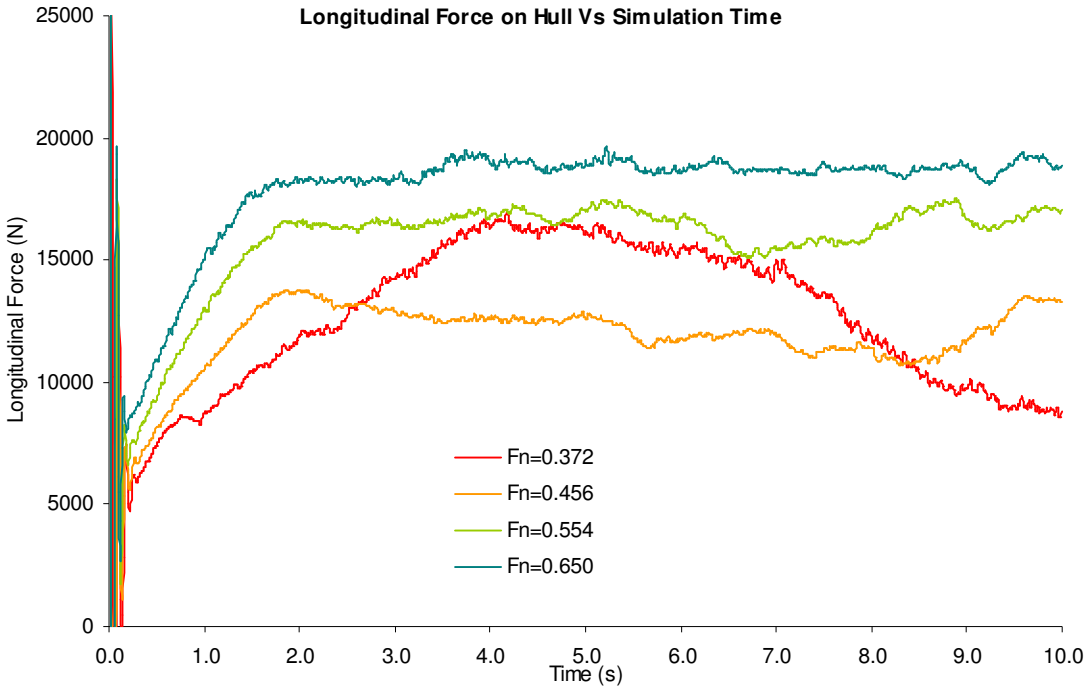

Figure: E.1

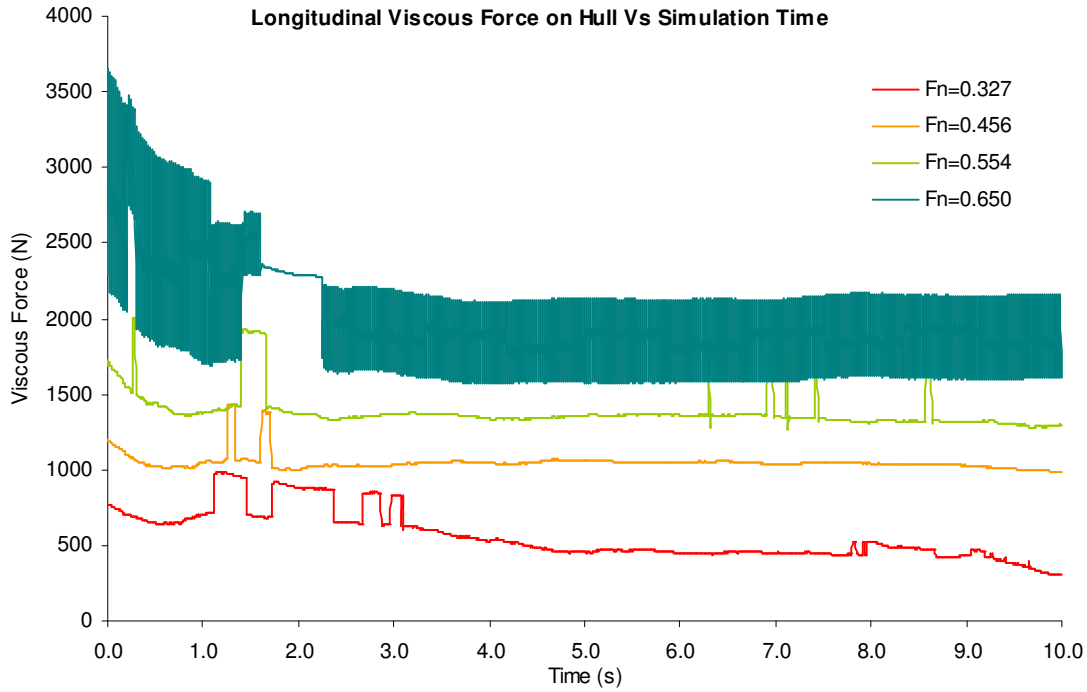

Figure: E.2

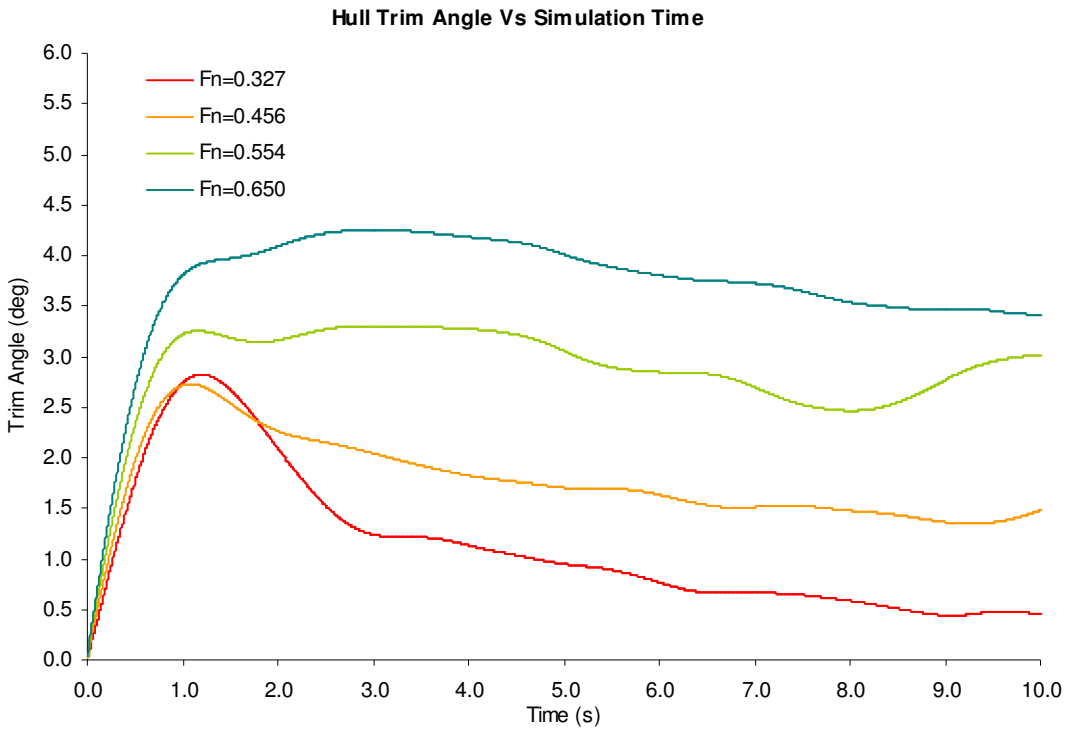

Figure: E.3

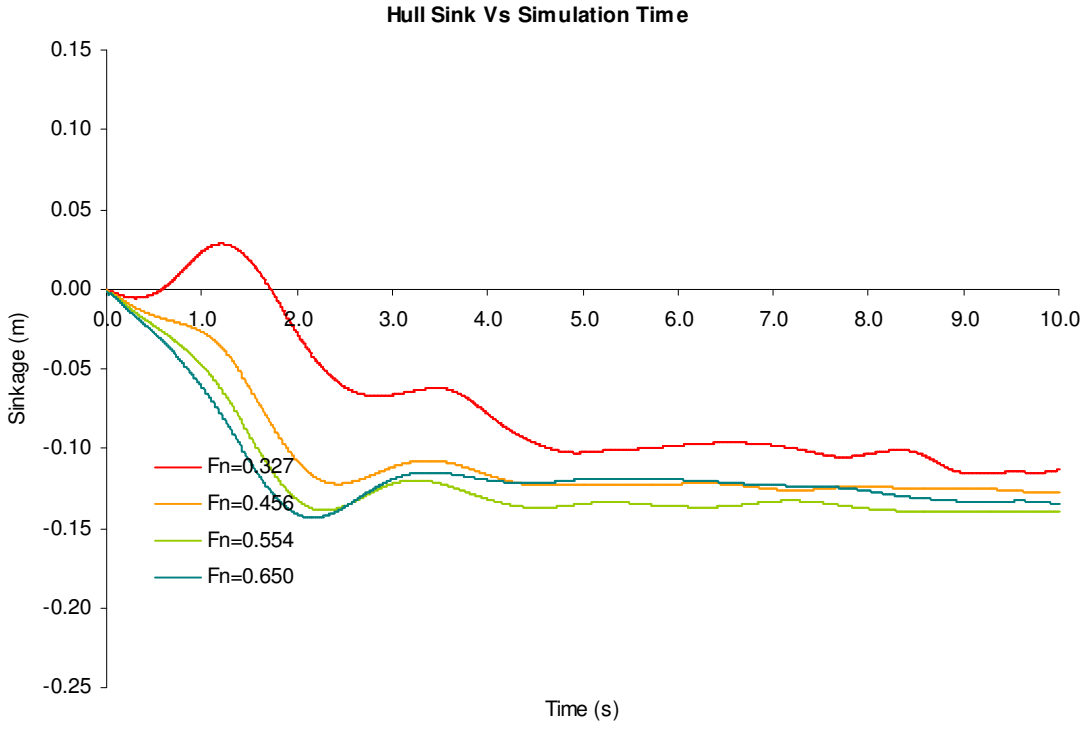

Figure: E.4

Appendix F

Bi-Wigley Catamaran: Sink and Trim Analysis in Still Water

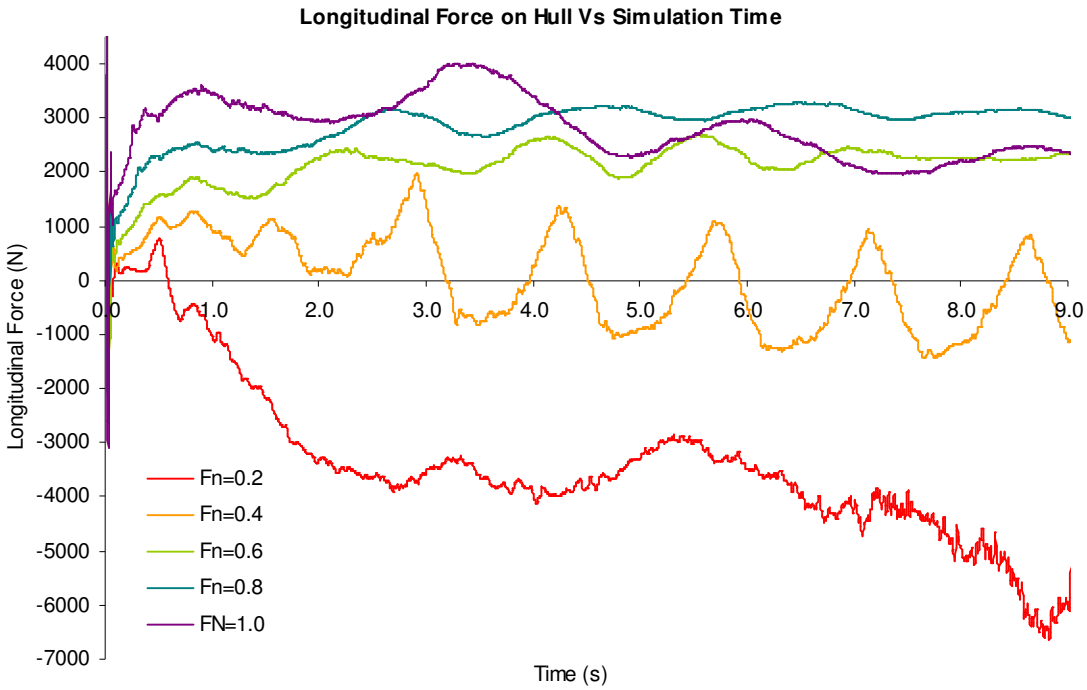

Figure: F.1

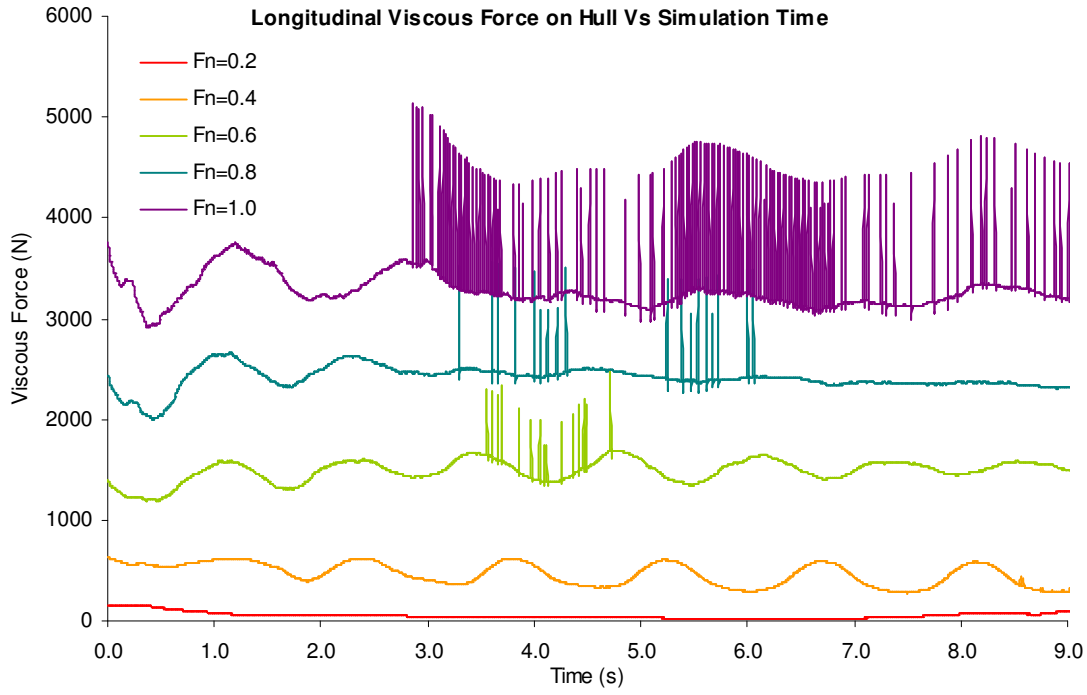

Figure: F.2

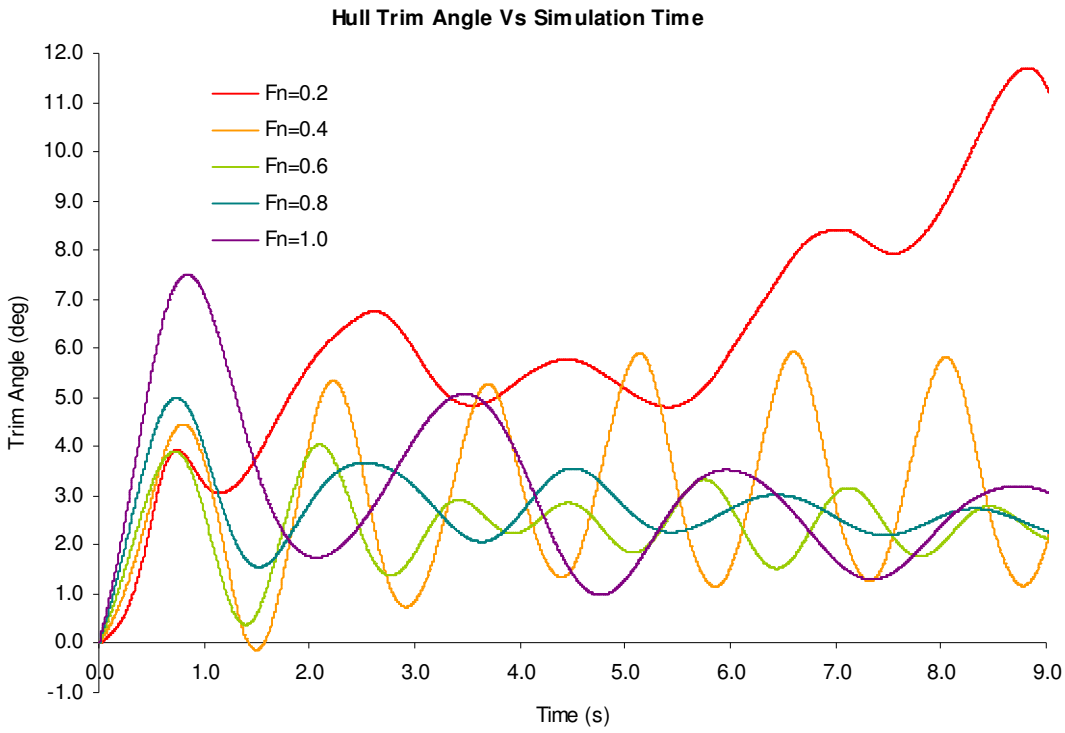

Figure: F.3

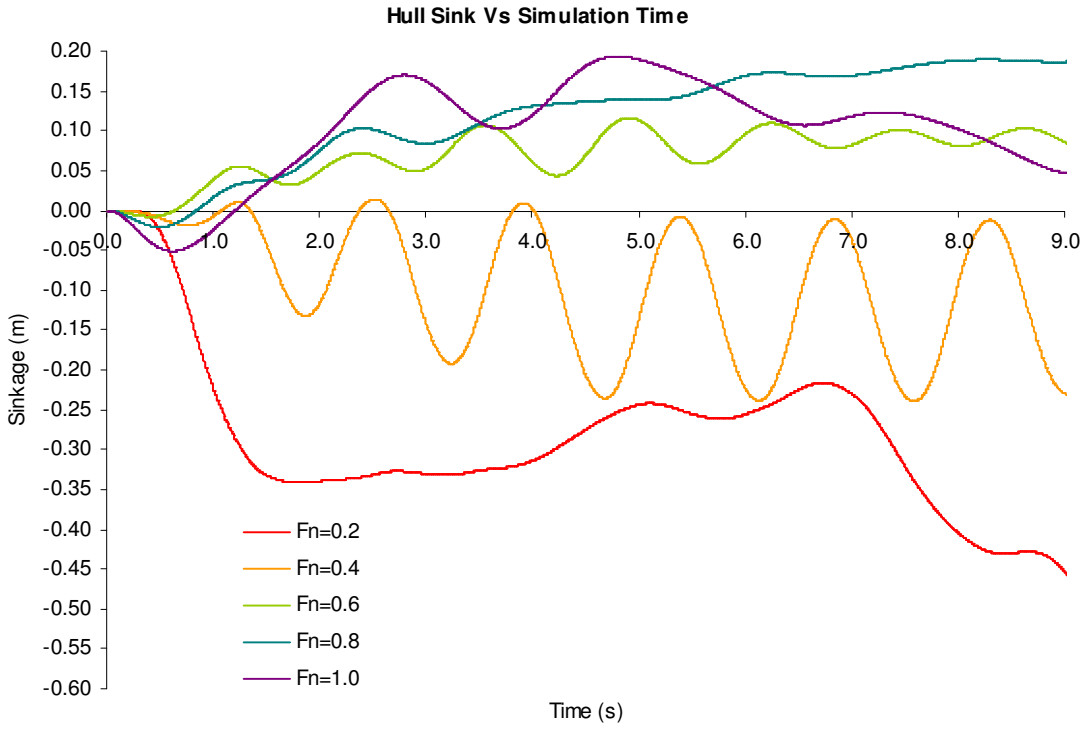

Figure: F.4